Using the Digital Shoreline Analysis System (DSAS) to Analyze Changes in Shoreline Position Caused by Seawalls Along a Section of Oregon's Coast

by

Melina Bennett

A Thesis Presented to the
FACULTY OF THE USC DORNSIFE COLLEGE OF LETTERS, ARTS AND SCIENCES
UNIVERSITY OF SOUTHERN CALIFORNIA
In Partial Fulfillment of the
Requirements for the Degree
MASTER OF SCIENCE
(GEOGRAPHIC INFORMATION SCIENCE AND TECHNOLOGY)

August 2021

For
My Parents,
Everyone who believed in me,
And Mr. Bowie – just keep swimming

Acknowledgements

I would like to thank my advisor, Dr. Fleming, for his help and guidance with this project as well as his patience and understanding when life interfered with this project. I would also like to thank my committee members, Dr. Wilson and Dr. Marx, as well as Dr. Bernstein for their feedback and guidance.

Table of Contents

List of Figures

List of Tables

List of Abbreviations

DEM	Digital Elevation Model
DSAS	Digital Shoreline Analysis System
EPR	End Point Rate
GIS	Geographic Information System
HWL	High Waterline
IPCC	Intergovernmental Panel on Climate Change
LiDAR	Light Detection and Ranging
LLC	Lincoln Littoral Cell
LRR	Linear Regression Rate
MHHW	Mean Higher High Water
MHW	Mean High Water
MIR	Middle Infrared
MNDWI	Modified Normalized Difference Water Index
MSL	Mean Sea Level
NAIP	National Agriculture Imagery Program
NAVD88	North American Vertical Datum of 1988
NDWI	Normalized Difference Water Index
NIR	Near-infrared
NOAA	National Oceanic and Atmospheric Administration
NOS	National Ocean Service
NSM	Net Shoreline Movement
PDO	Pacific Decadal Oscillation

SCE	Shoreline Change Envelope
SLR	Sea Level Rise
SPS	Shoreline Protection Structure
SWIR	Short-wave Infrared
USGS	United States Geological Survey
WLR	Weighted Linear Regression Rate

Abstract

The Lincoln Littoral Cell (LLC) contains a 24 km stretch of coastline along Oregon's central coast. Nearly 50% of the LLC's coastline has been armored with shoreline protection structures (SPSs), mainly riprap and seawalls. SPSs are constructed to reduce damage to coastal developments caused by breaking waves, flooding, and sediment erosion. Although the SPSs are meant to protect the coast from erosion, they can ultimately cause erosion adjacent to the structure or further down shore. Future projections and models show an increase in frequency of large storm systems that generate larger than average waves and water levels, resulting in increased erosion and flooding. This project utilizes the USGS's ArcGIS add-on, Digital Shoreline Analysis System (DSAS), to analyze digitized shoreline positions from 1997 to 2016. Visual analysis shows that while on average the shoreline is accreting at a rate of 0.32 m/yr, there is localized erosion adjacent to 53% of the SPSs. Future policies regarding the placement and build of SPSs should take into consideration the long-term negative effects of these structures.

Chapter 1 Introduction

Shoreline protection structures are generally constructed to protect buildings and other structures from damage caused by breaking waves. But as sea levels rise and the frequency of storm surges increase, it is becoming more apparent that these structures are interfering with the natural coastal processes that govern beach morphology. This interference can lead to an increase in erosion rates further along the shoreline. This study used shorelines extracted from aerial imagery and Light Detection and Ranging (LiDAR) derived digital elevation models (DEMs) to analyze changes in shoreline position along a heavily armored coastline in central Oregon.

1.1. Coastal Processes and Protection Structures

Coastal erosion due to sea level rise is a growing threat to coastal communities. The Intergovernmental Panel on Climate Change (IPCC) estimates that sea levels could rise anywhere from 0.28 to 0.98 m in the next 80 years depending on location (IPCC 2013). With over half a million people living along Oregon's coast, an increase in sea level will expose more people and structures to coastal hazards including saltwater inundation, flooding, and damages to buildings caused by sediment erosion (NOAA 2021c). Because of this, erosion mitigation efforts in the form of shoreline protection structures (SPSs) have been put into place to protect coastal developments from erosion. Man-made SPSs are a relatively short-term solution and can cause erosion adjacent to the SPSs themselves.

1.1.1. Coastal Processes

The simplified definition of the shoreline is the boundary between water and land. Although this seems simple enough, there are many factors that influence the position of this boundary such as water level and sediment transport (Boak and Turner 2005). Because the shoreline cannot be easily defined, shoreline proxies are often used in shoreline analysis. There are two types of shoreline proxies, visible and datum based. Visible proxies include alongshore features that are easily seen and include features such as a vegetation line, the top or base of a cliff, erosion scarp and the wet/dry sediment boundary or high-water line (HWL) (Boak and Turner 2005). Datum based shorelines use an averaged high or low water-level at a given location. These datums are calculated by averaging the value of high- or low-water levels recorded by a water gauge over a 19-year period known as the tidal datum epoch. NOAA calculates tidal datums, which includes data such as mean high water (MHW), mean sea level (MSL), and others, for each epoch. The current epoch uses data collected between 1983 and 2001. The next tidal datums for the epoch spanning from 2002 to 2020 are set to be released in 2025 (NOAA 2021f). Standard water level datums are calculated for MHW, mean higher high water (MHHW), mean low water (MLW), and mean lower low water (MLLW). Figure 1 shows the position of the tidal datums relative to the shore.

A littoral cell is defined by the natural cycle of fluctuating sediment loss and deposition. Specifically, a littoral cell is a segment of coastline that begins at a point where sediment is introduced and ends where sediment is deposited (Davidson-Arnott 2010; van Rijn 2011). Sediment introduced by rivers and cliff erosion are common sources of input into the sediment budget, while sediment that is transported and deposited offshore onto the continental shelf removes sediment from the sediment budget (Davidson-Arnott 2010). Littoral cells are not a closed system and sediment can be exchanged between adjacent cells (Anderson et al. 2018; Davidson-Arnott 2010). Seasonal variabilities, influenced by tides and storm surges, redistribute the sediment from the beach to nearshore sediment stores and vice versa (van Rijn 2011).

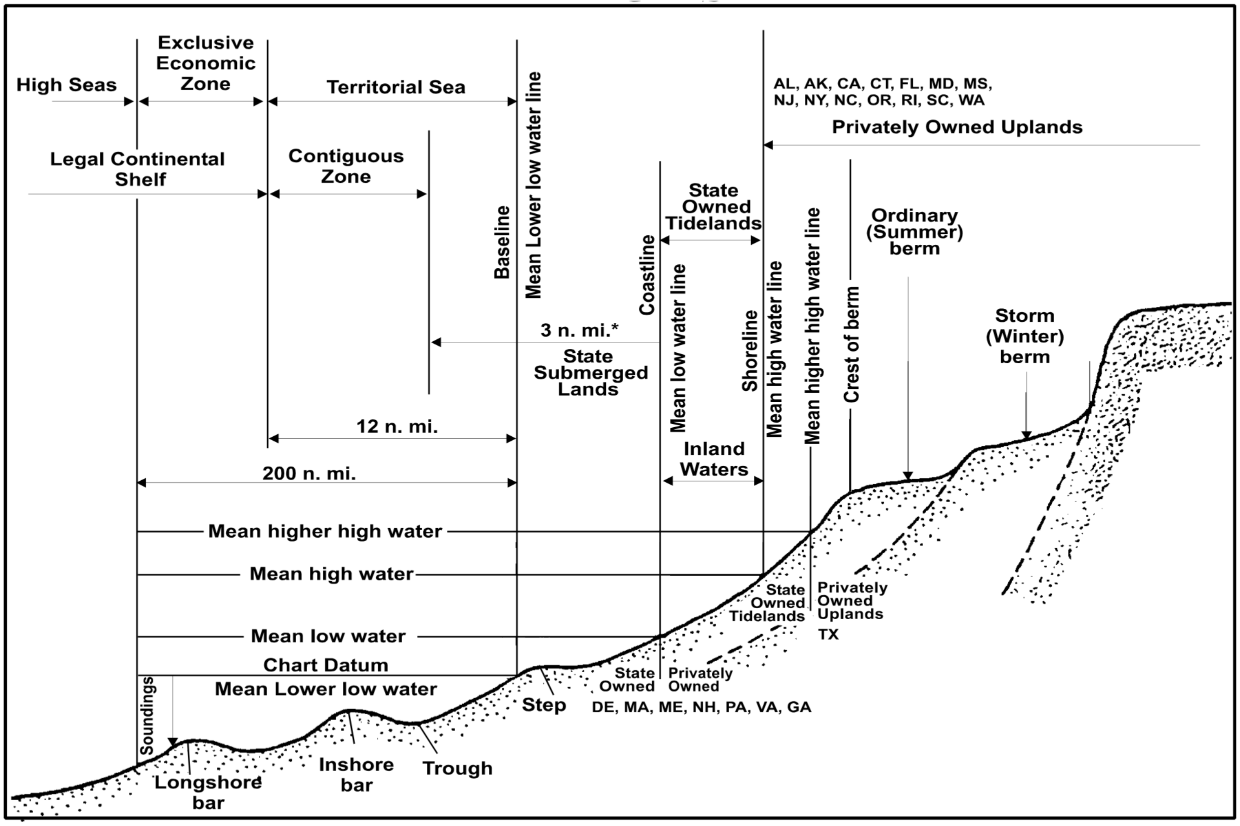

Figure 1. Cross shore profile depicting the difference in tidal datums in relation to the shore (Gill at al. 2001).

Coastal erosion affects the coastal zone by permanently removing sediment from the sediment budget. There are many natural and anthropogenic factors that contribute to the onset of coastal erosion including large storm systems, damming of rivers, and coastal development. One of the greatest influences is sea level rise (SLR). As sea levels rise, areas at higher elevations are increasingly exposed to powerful waves and flooding during large storm systems (van Rajin 2011).

There are several processes that influence changes to regional sea level. Some of these include an increase in the temperature of ocean waters causing thermal expansion, melting of glaciers and ice sheets, and vertical movement of the Earth’s crust due to tectonic or volcanic activity and isostatic adjustment caused by the melting of glaciers or sediment loading (Cazenave and Cozannet 2014). The Earth has a natural cycle of warming and cooling that regulates these factors. Even though SLR due to warming trends are naturally part of this cycle, the rate at which this is occurring is increasing (IPCC 2013). This increased rate is concerning because this will expose more people living along to coast to hazards such as flooding and damage to infrastructure and cultural assets (Reguero et al 2018).

Coastal erosion and SLR are just two factors that influence shoreline variability. Shoreline variability refers to the cycles of progradation and retrogradation of the shoreline that can occur temporally from tens of years to centuries (Stive et al. 2002). There are many other natural and anthropogenic factors that contribute to the shoreline variability. Some of these include wave and tide conditions, availability of sediment, geologic setting, shore nourishment, coastal structures, and natural resource extraction (Stive et al. 2002).

One of the natural influences on shoreline variability along the Oregon Coast are the occurrences of El Niño and La Niña events. The El Niño phenomenon occurs when the temperature of equatorial surface water in the Pacific rise above average, or below average for La Niña (NOAA 2021a). El Niño events culminate in larger than average storm surges, wave energy, and an increase in flooding events, all of which cause higher than average erosion rates (Barnard et al. 2015). Shorelines located between headlands generally have little to no erosion, but during El Niño events there is a greater rate of erosion that occurs at the southernmost sections and along the north side of inlets as shown in Figure 2. An increase in water level is another characteristic of El Niño events. During major El Niño events, water levels can increase by up to 0.4 m (Komar, Allan, and Ruggiero 2011). El Niño events occur every 3 - 5 years with major events occurring every 20 years, shown in Figure 3 (NOAA 2021a, Cai et al. 2014). The last notable El Niño event occurred over the winter between 2015 and 2016. Under current anthropogenic warming trends, extreme El Niño events are projected to double from one in every 20 years to one in every 10 by 2090 (Cai et al. 2014).

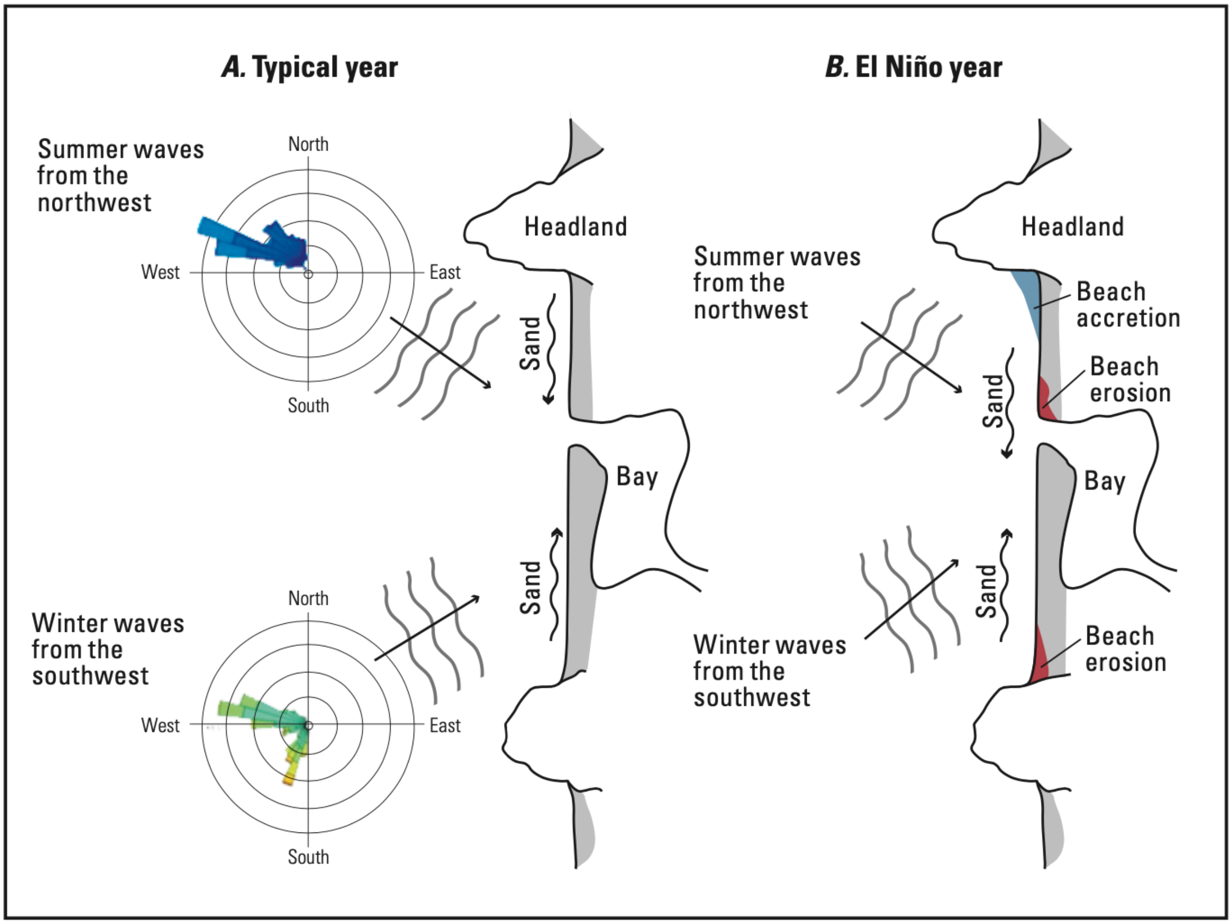

Figure 2. Diagram showing the typical equilibrium in sediment transport between summer and winter (a) and where greater wave energies during El Niño years causes erosion in headland bound shorelines (b) (Ruggiero et al. 2013).

At a larger time scale, the Pacific Decadal Oscillation (PDO) is characterized by monthly averaged sea surface temperature anomalies in the North Pacific. The PDO is influenced by multiple oceanic processes from the northern and tropic regions of the Pacific, such as El Niño and others (Newman et al. 2016). Warm and cool phases of the PDO alternate every 20 years and because the PDO reflects multiple processes, it does not have as apparent characteristics like large storm systems with El Niño.

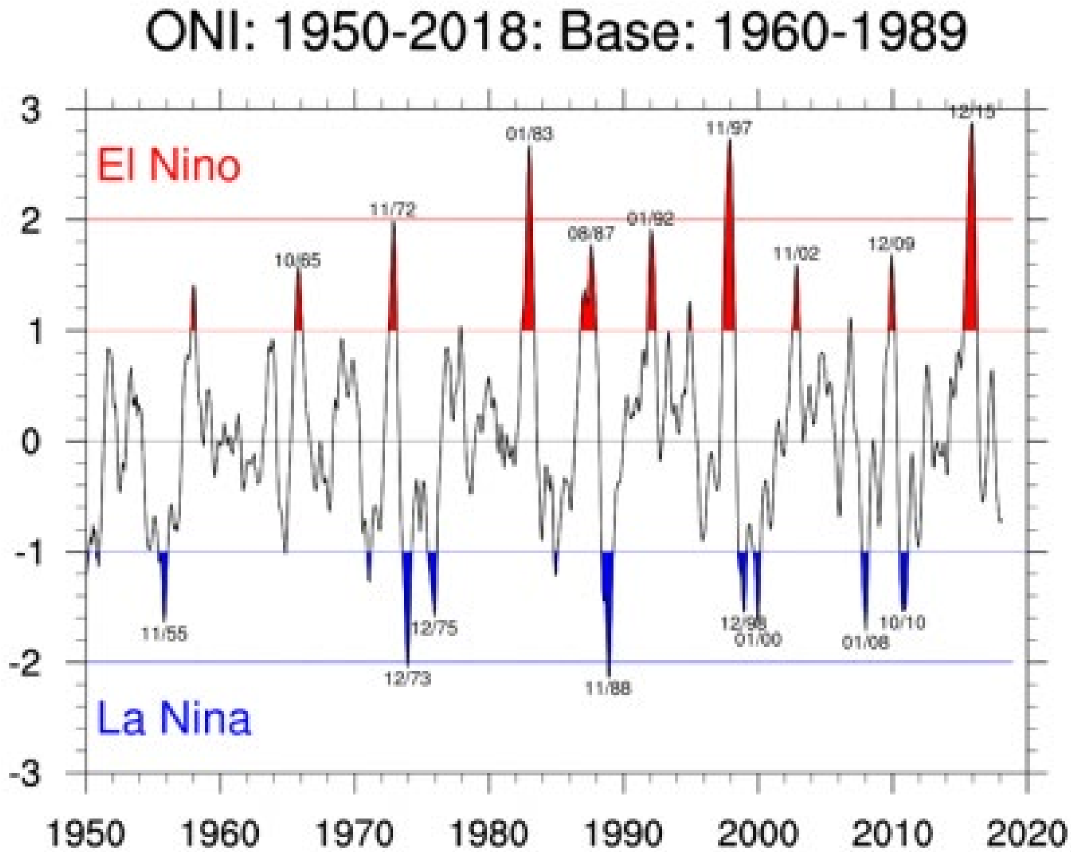

Figure 3. Occurrence of El Niño and La Niña from 1990 to present, the clored peaks in the graph show when moderate and extreme El Niño and La Niña events have occurred. (Trenberth 2020).

1.1.2. Erosion Mitigation Structures

Man-made structures, such as seawalls, are commonly constructed to mitigate the effects of coastal erosion. Although these structures are used to inhibit erosion in specific areas, research shows that they interfere with the sediment transport within a littoral cell. This can prevent sediment from entering and moving within the system as well as causing greater erosion adjacent to the structure and/or further down the shoreline (Kraus and McDougal 1996; van Rijn 2011).

Seawalls are structures that run parallel to the shoreline and are generally constructed using concrete. They are designed to prevent landward retreat of the shoreline by reflecting or dissipating the energy of breaking waves (Kraus and McDougal 1996). Ripraps are a type of seawall consisting of large chunks of rock or concrete that are piled along the shoreline to dissipate the energy of breaking waves (Hiller, Lia, and Aberle 2019). Examples of a seawall and riprap installed along the Oregon Coast are given in Figures 4 and 5 respectively. The length and location of where the seawall is constructed determines the effectiveness of the structure (Weggel 1988). Seawalls constructed close to the active shoreline have a greater influence on sediment transport by preventing the sediment behind the wall from entering into the system and causing erosion at either the base of the wall and/or where the wall ends (Weggel 1988). Because placement of these hard structures is critical to their effectiveness and varies depending on the beach type, any negative effects might not be noticeable in the short term (Pilkey and Wright 1988). The dynamic nature of the sea level and shoreline position prevent these structures from permanently occupying an ideal location to inhibit coastal erosion. This fluctuation can ultimately lead to unintended alterations in shoreline morphology.

Figure 4. Installed seawall in Oregon (DLCD 2021).

Figure 5. Newly installed riprap in Lincoln County, Oregon (Kauffman 2018).

1.2. **Study Area**

The Oregon coast lies on top of the Cascadia Subduction Zone where the Juan de Fuca oceanic plate is subducting under the North American continental plate. The Cascadia Subduction Zone was thought to be inactive due to the lack of seismic activity, but it is now believed that the two plates are locked together (Komar and Shih 1993). As a result of the strain due to the lock, the southern Oregon coast is being uplifted at a rate faster than eustatic SLR (Komar and Shih 1993). The northern and central sections of the Oregon coast are being uplifted at a slower rate than eustatic SLR resulting in a regional SLR of 1 to 2 mm/yr (Ruggiero et al 2013).

Located along Oregon's central coast, the Lincoln Littoral Cell (LLC) stretches 24 km from Cape Foulweather north to Cascade Head. The LLC contains the most developed section of Oregon's coast. Roughly 50% of the shoreline is armored with 244 SPSs built to protect these developments (Gardner, 2015; Good 1992). Riprap and seawalls are the two types of SPSs constructed along the shoreline (Good 1992). The extent of the constructed SPSs is shown in Figure 6.

The majority of the beaches within the LLC are backed by cliffs comprised of Pleistocene sands and gravel (Shih and Komar 1994). The sediments on the southern beaches are fine-grained and increase in size north towards Siletz Spit and then gradually decrease in size further north to Cascade Head, shown in Figure 7 (Komar and Shih 1993). This is of importance because sediment size influences erosion rates. Dissipative beaches that consist of finer grained sand, like that along Lincoln City, have a smaller slope resulting in lower energy wave swash (Komar and Shih 1993). Reflective beaches consist of gravel and have a steeper profile resulting in higher energy wave swash (Komar and Shih 1993). There are two small rivers that drain into the ocean within the LLC, the Salmon and Siletz Rivers. The Salmon River contributes a minor amount of sediment because of its small size whereas the Siletz River is likely a sediment store with marine sediment being deposited within the Siletz estuary. The main source of sediment within the LLC is a result of cliff erosion (Shih and Komar 1994). With the majority of the beaches in the LLC backed by cliffs, the 244 SPSs are preventing an estimated 39% of the sediment supply from entering the sediment budget (Good 1992).

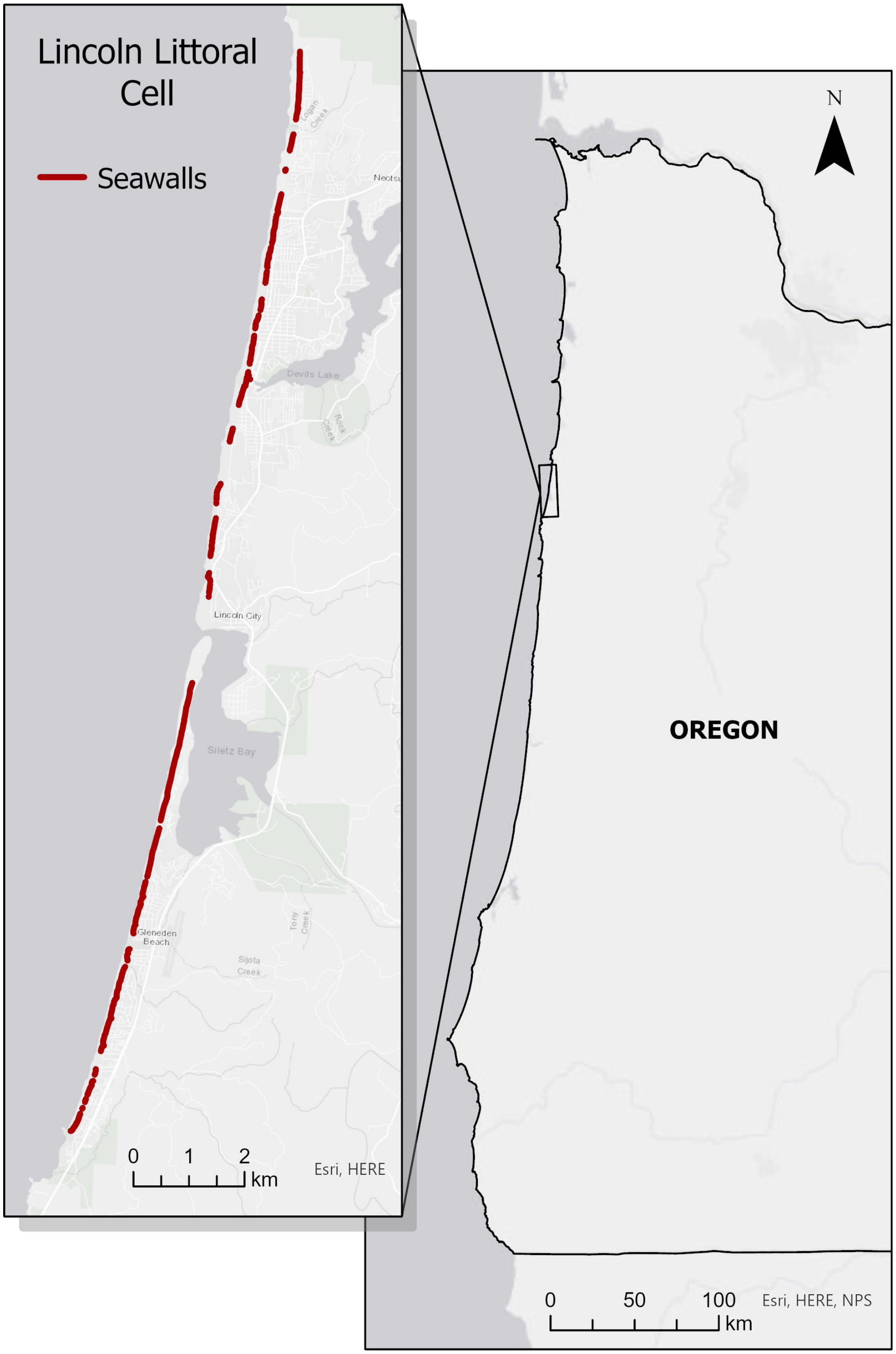

Figure 6. Location of the LLC relative to the Oregon coast. Red lines represent the locations of seawalls.

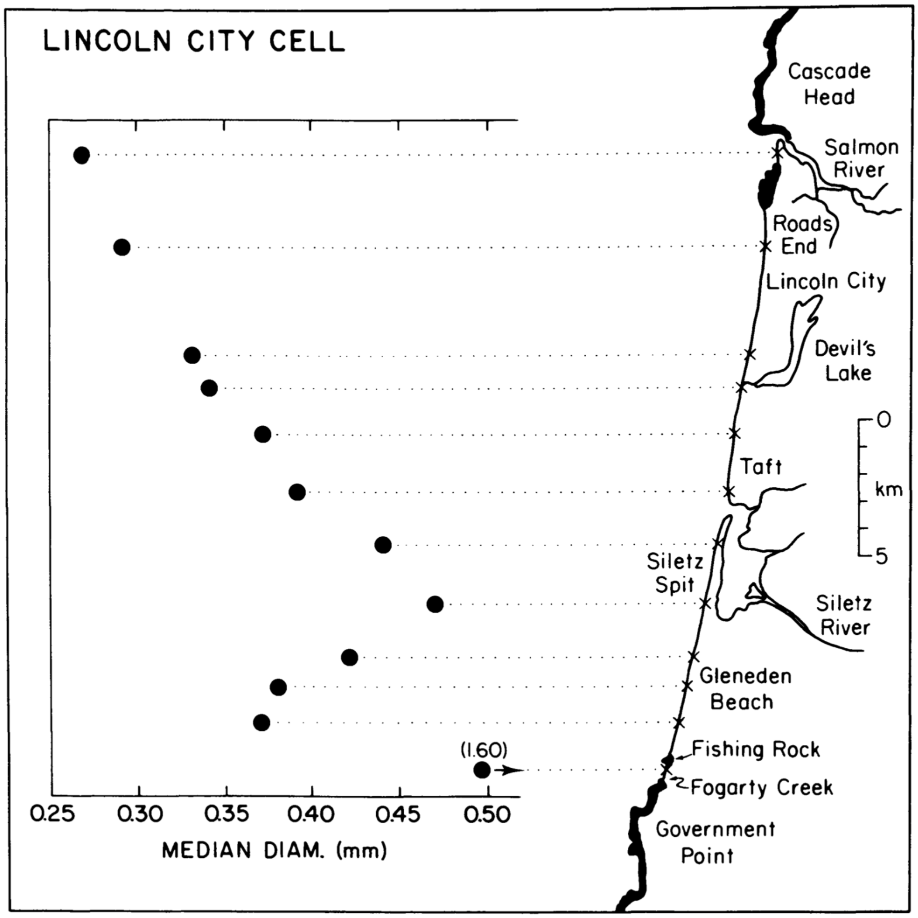

Figure 7. Sediment size distribution along the LLC (Shih and Komar 1994).

1.3. **Objectives**

The LLC, located along Oregon's Central Coast, is heavily armored with seawalls and riprap. These structures were constructed to protect the ground under and around infrastructure from eroding by dissipating and reflecting wave energy. But when water levels and wave energy are greater than average, like during El Niño events, erosion can occur at the base, either end of the structure, and further down the shore. The rate of major El Niño events are increasing and in conjunction with SLR, the structures will be exposed to larger waves and flooding more frequently. This will eventually lead to damaging the structure and infrastructure it was meant to protect. Understanding exactly how the shore morphology responds to the installed SPSs can help coastal planners and engineers with future planning and assessments on previously installed structures. The goal of this study is to determine if shoreline change analysis can be used to detect erosion caused by seawalls along the LLC.

Chapter 2 Related Work

This chapter reviews literature related to the effectiveness of SPSs, discusses previous shoreline monitoring studies within the LLC, and compares shoreline change analysis methods.

2.1. Shoreline Protection Structures

The various methods for coastal erosion mitigation have been reviewed by van Rijn 2011 and Pranzini, Wetzel, and Williams 2015. They found that groins and seawalls are the most common shoreline protection structures and both structures cause greater erosion elsewhere in the littoral cell. Because of this, most countries are moving towards erosion mitigation methods that do a better job of conserving the surrounding environments. This includes taking into consideration the sediment transport within the littoral cell because different shoreline protection structures work differently depending on the shoreline type (Pranzini, Wetzel, and Williams 2015).

Darwish et al. (2017) compare shorelines along the Nile Delta from 1945 to 2015. In the late 1960s a dam was built upstream, significantly reducing the sediment output of the Nile River. This drop in the sediment supply resulted in erosion focused immediately down-drift of channel mouths. To remedy this, seawalls were constructed in the early 2000s (Darwish et al. 2017). The construction of the dam and seawalls has had a large impact on the shorelines; Figure 8 shows how these SPSs altered the shoreline position, and that erosion is focused adjacent to the structures (Darwish etl al. 2017).

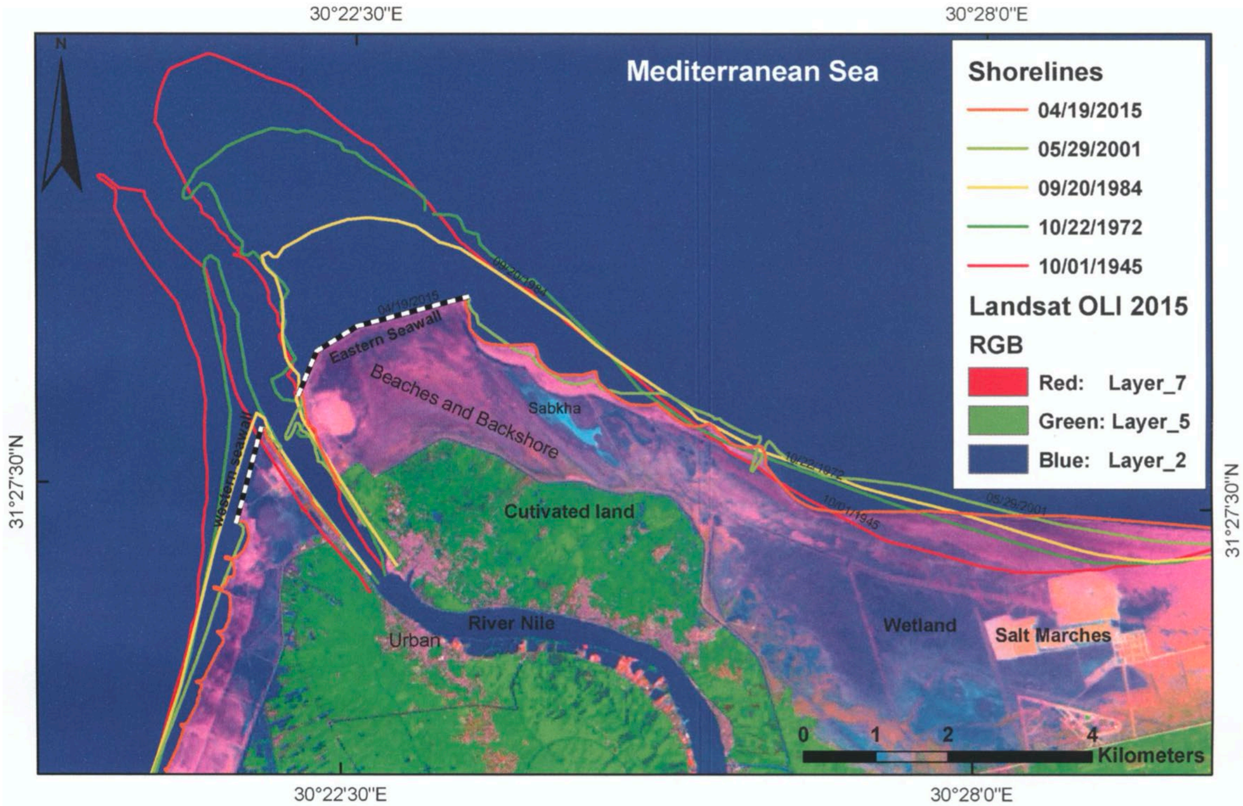

Figure 8. Change in shoreline position near a channel mouth of the Nile River showing where erosion is focus after the construction of two seawalls on either side of the channel mouth (Darwish et al. 2017).

Along a section of the Northern Tuscany Coast in Italy, shoreline protection structures have been used to mitigate erosion caused by rising sea levels, reduced sediment output from three nearby rivers, and the construction of harbors (Pranzini et al. 2018). In this study, Pranzini et al. (2018) follow the construction of groins, detached breakwaters, and seawalls along the coast. They map the changes to the shoreline position from 1878 to 2017 using historical maps, ortho-rectified aerial photographs, and satellite imagery. The majority of these structures were constructed in response to increased erosion down-drift of an older structure. The use of these hard structures is popular because they provide almost instantaneous results compared to long-term methods like sediment bypassing and beach nourishment (Pranzini et al. 2018). This is one of the only studies that specifically looks at the effectiveness of SPSs for the lifespan of the structure and discusses the benefits of switching to a more sustainable erosion mitigation method.

Although seawalls are known to have adverse effects on shoreline morphology, not much is known about how shorelines with seawalls will react to SLR. Beuzen et al. (2018) created a model to test how shorelines with seawalls will change due to SLR. The model projected the shoreline profiles with dissipative and reflective seawall structures to profiles without seawalls to compare the profile response to SLR. They found that with an increase in water level, shorelines with seawalls (dissipative and reflective) eroded similar volumes of sediment as shorelines with no protection but that the erosion was focused to areas adjacent to the seawall.

2.2. **Shoreline Monitoring Within the Lincoln Littoral Cell**

The majority of the shorelines within the LLC are heavily armored with riprap and seawalls. Because of the high wave energy and shoreline variability along Oregon's coast, previous studies have assessed the LLC's shoreline position, erosion hazards, wave climate, and current coastal policies.

2.2.1. SPSs and Shoreline Change Analysis

A thorough account of the LLC's SPSs and the regulations governing the alterations and construction of new structures is provided in Good's doctoral thesis (Good 1992). Good created a spatial database that included information on when the structures were built, sediment supply, erosion rates, and Oregon's policies on SPSs. The main goal of the thesis was to assess the implementation of shoreline protection policies. To quantify this, he looked at the effectiveness of the SPSs. Before the implementation of Goal 18, new development did not take future geologic and oceanographic hazards into consideration and built structures in less-than-ideal locations that eventually required SPSs. Assuming that most of the sediment supplied to the beach is from cliff erosion and using erosion rates, Good calculated that the existing SPSs prevent about 39% of the annual sediment supply from entering the sediment budget. This is a good argument on the probability that SPSs will have a negative effect on the surrounding shoreline within the LLC but there is no direct spatial analysis testing this claim.

In a similar concept to Good's analysis, Priest (1999) used erosion rates to predict areas that would be affected by coastal erosion. The shorelines of the LLC were assessed for erosion hazards to project property damage that could occur within a 60-year time frame. Shorelines with SPSs were assumed to have the same erosion rate as adjacent unprotected shorelines unless the SPSs met a set of criteria. The criteria required the structures to be at least 150 m in bluff-backed shorelines or 300 m for dune-backed shorelines, have been standing undamaged for at least 10 years, and could not have an active landslide located behind it (Priest 1999). There is not much discussion on the SPSs that met the above criteria or if there were any erosion hazards that were a direct result of existing SPSs.

Allan, Komar, and Priest (2003) used shoreline position data from littoral cells north and south of the LLC to determine any long-term trends in shoreline position. Although this study did not include the LLC specifically, the authors were able to conclude that long-term shoreline change for the entire coast of Oregon was negligible. They determined that the short-term shoreline variability caused by El Niño and La Niña events should be the main consideration when assessing erosion hazards and setback distances for constructing new developments.

More recently, the United States Geologic Survey (USGS) used historical aerial photographs, National Ocean Service (NOS) topographic sheets (T-sheets), and LiDAR to calculate the short- and long-term shoreline change rates along the coastlines of Oregon and Washington (Ruggiero et al. 2013). Shorelines were digitized from the source material and then analyzed in USGS's ArcGIS add-on Digital Shoreline Analysis System (DSAS). Short-term change rates are determined by calculating the endpoint, which is the change in shoreline position divided by the time between the data sets. Long-term change rates required at least four years of data and is determined by the slope of the linear regression. Both short- and long-term change rates are calculated because some shorelines do not change in a linear trend and linear regression cannot account for these non-linear trends. Short- and long-term change rates for the LLC were determined to be -0.3 ± 0.1 m and 0.1 ± 0.5 m respectively. The short-term change rate was attributed to the possibility that sediment supply has been interrupted due to the presence of SPSs (Ruggiero et al. 2013). The goal of this study was to determine shoreline change rates of large sections of coastline along the pacific northwest, making the scope of this study too large to be able to examine how SPSs specifically affect the shoreline within the LLC. This project uses a similar methodology as this study to calculate shoreline change rates.

2.2.2. Extreme Storms and Wave Variability

Over the winters of 1997-98 and 1998-99 four extreme storms, classified by generating deep water significant wave heights greater than 10 m, occurred in the Eastern North Pacific (Allan and Komar 2002). The 1997-98 winter was classified as an El Niño with one extreme storm in November that had a storm surge of 0.41 m bringing the total water level to 0.81 m. There were three extreme storms the following La Niña winter. The largest storm surge recorded from the three storms was 0.61 m, because water levels are lower during La Niña events compared to El Niño, the total water level reached 0.82 m (Allan and Komar 2002). Alan and Komar (2002) looked into the deep-water wave heights for the previous 25 years and concluded that large storms like this are occurring more frequently with increasing strength. Allan and Komar (2006) revisited their 2002 study to add to and update their predictions. They found that the general trend in increased wave height continues. This time they noted the connection to the PDO and that it was shifting to a predominantly La Niña phase suggesting a decrease in overall erosion.

More recent studies that created models on deep-water wave height disagree with Allan and Komar's (2006) prediction of increasing wave heights. Erikson et al. (2015) used two different climate models to simulate surface winds and create wave height predictions. They found that predicted wave heights should decrease along the Oregon coast but note that among other similar studies there are some contradictions to these findings. They recommend a future study that takes into account different climate projections with more iterations to capture a wider range of conditions that influence wave height.

Trends in shoreline variability have been identified in conjunction with events such as El Niño, but such events do not account for trends that occur at larger time scales. Anderson et al. (2018) created a model of wave energy off of the Oregon Coast to try to identify any relationships between shoreline variability and multidecadal oceanic phenomena. They were able to identify a direct correlation between the modeled wave energy and the PDO index. This was observed in Pacific City, Oregon (located in the littoral cell just north of the LLC) between 1970 where riprap were installed due to high erosion rates and 1984 when the riprap were completely buried by sand (Allan, Komar, and Priest 2003; Anderson et al. 2018). Anderson et al.'s (2018) model showed a decrease in wave energy coinciding with a cool phase of the PDO in the 1970s and an increase in wave energy in the 1980s during a warm phase of the PDO. This correlation supports Allan and Komar's (2006) observations that shifts in the PDO result in either increased El Niño or La Niña events which directly correspond to erosion rates.

2.2.3. Coastal Policy

In 1967 the Beach Bill was passed requiring that the beaches along Oregon's entire coast are accessible to the public for free. The Oregon Statewide Planning Goal 18, Beaches and Dunes (OAR 660-015-0010) was created to help ensure that the Beach Bill is maintained. Goal 18 provides details on where developments can be constructed along the coast. Additionally, Goal 18 requires SPSs to have a permit and outlines the requirements for a tax lot to be eligible for a SPSs. One of the requirements is that the development on the lot has to have been built before January 1, 1977. Gardner (2015) assessed these policies and all oceanfront tax lots along the Oregon Coast to provide ideas on how to improve the policies and permitting regulations. At the time of the report, tax lots were only assessed based on adjacent structures, SPSs under 50 ft did not require a geologic report, and little to no plan was in place to address situations where development might become compromised due to erosion. To address this, Gardner (2015) recommends that all permits require a geologic and hazard assessment, impacts of the SPSs be assessed for the entire littoral cell, and that there should be set design standards for constructing new SPSs and repairing old ones. This report highlights the fact that the current coastal policies do not take into account the future impacts of SLR, climate change, and the installed SPSs.

2.3. **Shoreline Extraction and Analysis**

There are several different methods when it comes to digitizing shoreline position depending on the source data. These sources can include historical shorelines from NOS T-

Sheets, georeferenced aerial and satellite imagery, LiDAR point clouds and DEMs. Once the shorelines are extracted, positional rate changes are able to be calculated and analyzed.

2.3.1. Proxy-Based Shoreline Extraction

To determine shoreline position, the boundary between the ocean and land needs to be identified and this can be accomplished by classifying each pixel as either land or water. This process can be automated by using different spectral bands to calculate an index and specifying a threshold that determines the values that represent land or water (Fisher, Flood, and Danaher 2016). There are many indices that have been created to distinguish between land and water with two the most commonly used ones being Normalized Difference Water Index (NDWI) and Modified Normalized Difference Water Index (MNDWI).

NDWI was introduced in 1996 by S. K. McFeeters and uses the green and near infrared (NIR) spectral bands to identify pixels representing water. This index is based off of the Normalized Difference Vegetation Index which uses the red and NIR bands to enhance vegetation features. NDWI enhances water features due to the fact that water has a high green and low NIR reflectance compared to vegetation and soil features (McFeeters 1996). The equation returns either a positive or negative value, with positive values indicating a greater green reflectance and therefor representing water (McFeeters 1996).

One of the issues with NDWI is that urban areas can have a NIR reflectance value that is close to its green reflectance, and this can result in urban areas having a NDWI value that is positive, falsely classifying it as water (Xu 2006). To address this Xu (2006) created the MNDWI that uses middle infrared (MIR) instead of NIR. Urban areas reflect more MIR than NIR resulting in values that will always be negative (Xu 2006).

Both NDWI and MNDWI only use two spectral bands to calculate the difference in reflectance values and depending on what other features, such as shadows, are in the image can result in misclassification (Feyisa et al. 2014). In a study using NDWI to identify pixels representing swimming pools in a residential neighborhood, McFeeters (2013) addressed the misclassification due to shadows by changing the threshold from 0 to 0.3. Multiple studies have compared the different water indices and concluded that the varying accuracies of each index is influenced by cloud cover, beach type, and landcover features (Fisher, Flood, and Danaher 2016; Kelly and Gontz 2018).

Once the water index has been calculated, the resulting raster images have two values that ideally denote either water or land. The shoreline position can then be extracted by converting the rasters to vectors. The resulting vectors will most likely need to be cleaned up to remove any lines that do not represent the shoreline (Sunder, Ramsankaran, and Ramakrishnan 2017).

2.3.2. Datum-Based Shoreline Extraction

Two methods for extracting shorelines from LiDAR data are the Profile and Contour methods. The Profile method utilizes LiDAR point cloud data and was first described by Stockdon et al. (2002). This method looks at a cross-shore profile and points that fall within one meter of either side of the profile. A datum-based shoreline position, such as MHW, is selected and the points ± 0.5 m are plotted with a regression line. The horizontal shoreline position and foreshore beach slope are determined by the slope of the regression line. This is repeated every 20 m along the shoreline.

The Contour method uses a DEM and adds a contour line along a specified elevation representing the shoreline position and is described in detail by Harris et al. (2006). The contour spatial analysist tool in either ArcGIS Pro or ArcMap can be used to add a contour line along a datum-based shoreline elevation, generally MHW. This elevation is used as the base contour value and the contour interval is set to a large arbitrary number. The contour feature class is edited to only include lines that represent the shoreline and remove any loops or breaks.

Although both of these methods use LiDAR data to extract datum-based shorelines, they do not necessarily place the shoreline in the same position. Ferris et al. (2018) compared these two methods to determine which one was more accurate. Shorelines were generated from the same LiDAR data using both methods. They concluded that there was an insignificant difference between the shoreline positions generated by the two methods. Comparing the methods, the Profile method requires programming knowledge, and can be time consuming but uses linear regression to calculate the shoreline position and slope. The Contour method is relatively quicker and easier to create but cannot extract shorelines where water levels are above MHW.

2.3.3. Combining Proxy- and Datum-Based Shorelines

NOS T-Sheets are historical records of shorelines that were mapped through surveys and aerial photographs using the HWL. Because these records date back to the 1800's, the HWL is still one of the most commonly used shoreline proxies (Moore, Ruggiero, and List 2006, Ruggiero et al 2013). Although the HWL is frequently used, there are uncertainties associated with its position relative to the recorded high-water level such as short-term fluctuations in wave energy (Ruggiero et al. 2013). This is reflected as an over-estimation of the shoreline. Another uncertainty is how the HWL is interpreted and digitized for shoreline analysis. Both Moore, Ruggiero, and List (2006) and Ruggiero et al. (2006) had multiple analysists draw the HWL from an aerial photograph to demonstrate the variability in HWL interpretation. The resulting offset between these shorelines from Moore, Ruggiero, and List (2006) are shown in Figure 9.

Just as the HWL overestimates the recorded high water-level, MHW datum-based shorelines underestimate the high water-level. This is because tidal datums are an average of high tide measurements at one location and fail to take into consideration alongshore variations in wave conditions and shore morphology (Ruggiero et al. 2013).

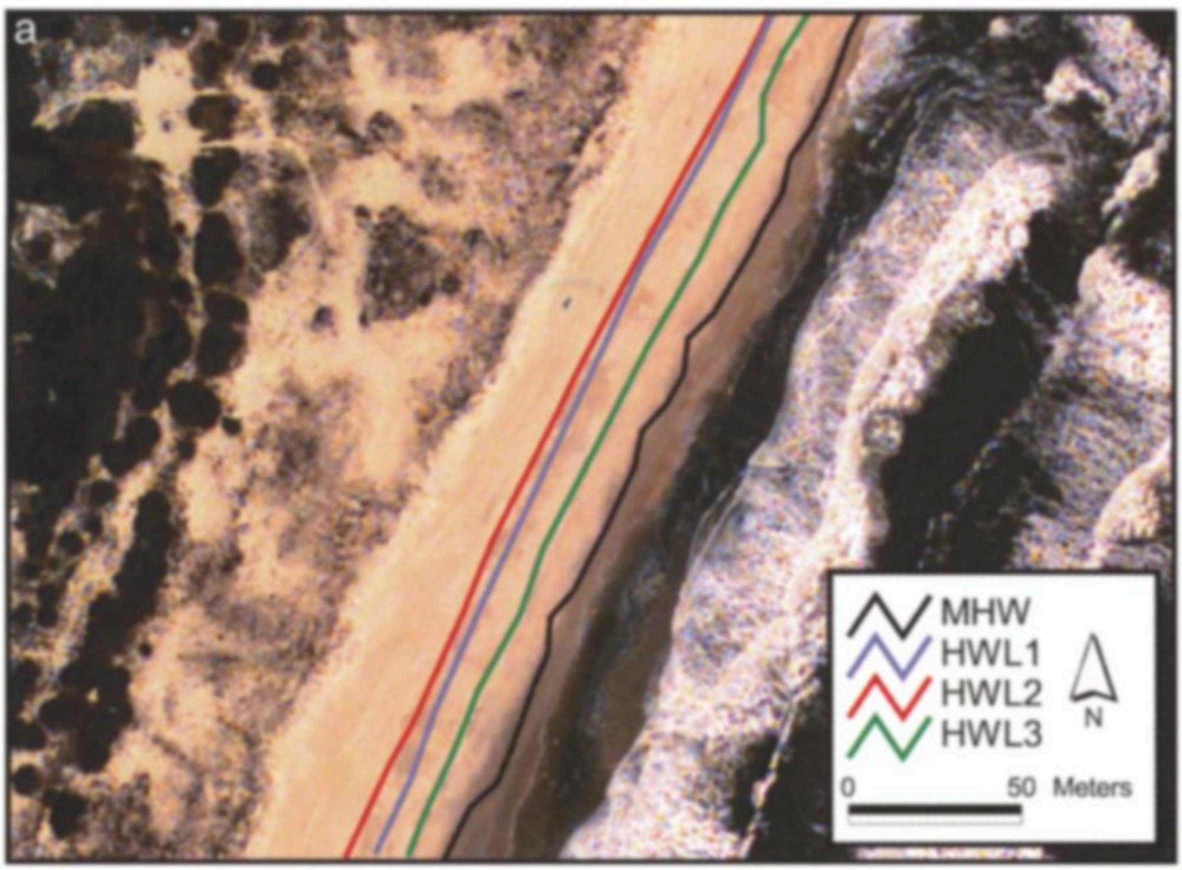

Figure 9. Difference in HWL position interpreted by three different analysists (Moore, Ruggiero, and List 2006).

Ruggiero and List (2009) recognized the offset of the HWL and MHW shorelines as a bias. They determined that the bias was a function of the water-level, foreshore beach slope, and the significant offshore wave heigh and period. Because all of these factors are easily measured or estimated they were able to create a proxy datum bias equation. Although these measurements are easily obtainable for current data, most historic data is not recorded at the same spatial and temporal resolution and therefore have uncertainties associated with them. Ruggiero and List (2009) used the proxy datum bias equation to derive equations to determine the long-term estimates for these factors as well as the uncertainty in the proxy datum bias equation. These equations allow for HWL and MHW shorelines to be used in the same analysis and are defined and discussed further in Section 3.2.

2.3.4. Shoreline Change Analysis

Shoreline change analysis calculates the rate at which the shoreline position moves over a period of time. This rate change can be calculated using various statistical methods including end point rate (EPR), linear regression (LLR), and weighted linear regression (WLR). Genz et al. (2007) compare nine statistical methods that have been used in shoreline change analysis to determine which method best represents the change rates for shorelines in Maui, Hawaii. Figure 10 shows the methods compared and the difference in how the regression line is fitted for each method using the same shoreline data (Genz et al. 2007). They concluded that all methods tested, except EPR, average of rates (AOR), and middle description length (MDL), are acceptable for shoreline change analysis. Specifically, if uncertainties are known, weighted least squares (WLS) and reweighted weighted least squares (RWLS) provide the best results. If uncertainties are unknown, the best method would be least absolute deviation (LAD), but ordinary least squares (OLR), reweighted least squares (RLS), and jackknifing (JK) could be used (Genz et al 2007). Each statistical method is explained in detail in Genz et al. (2007). This study uses the EPR, OLR (LRR), and WLS (WLR) as described in Section 3.3.3.

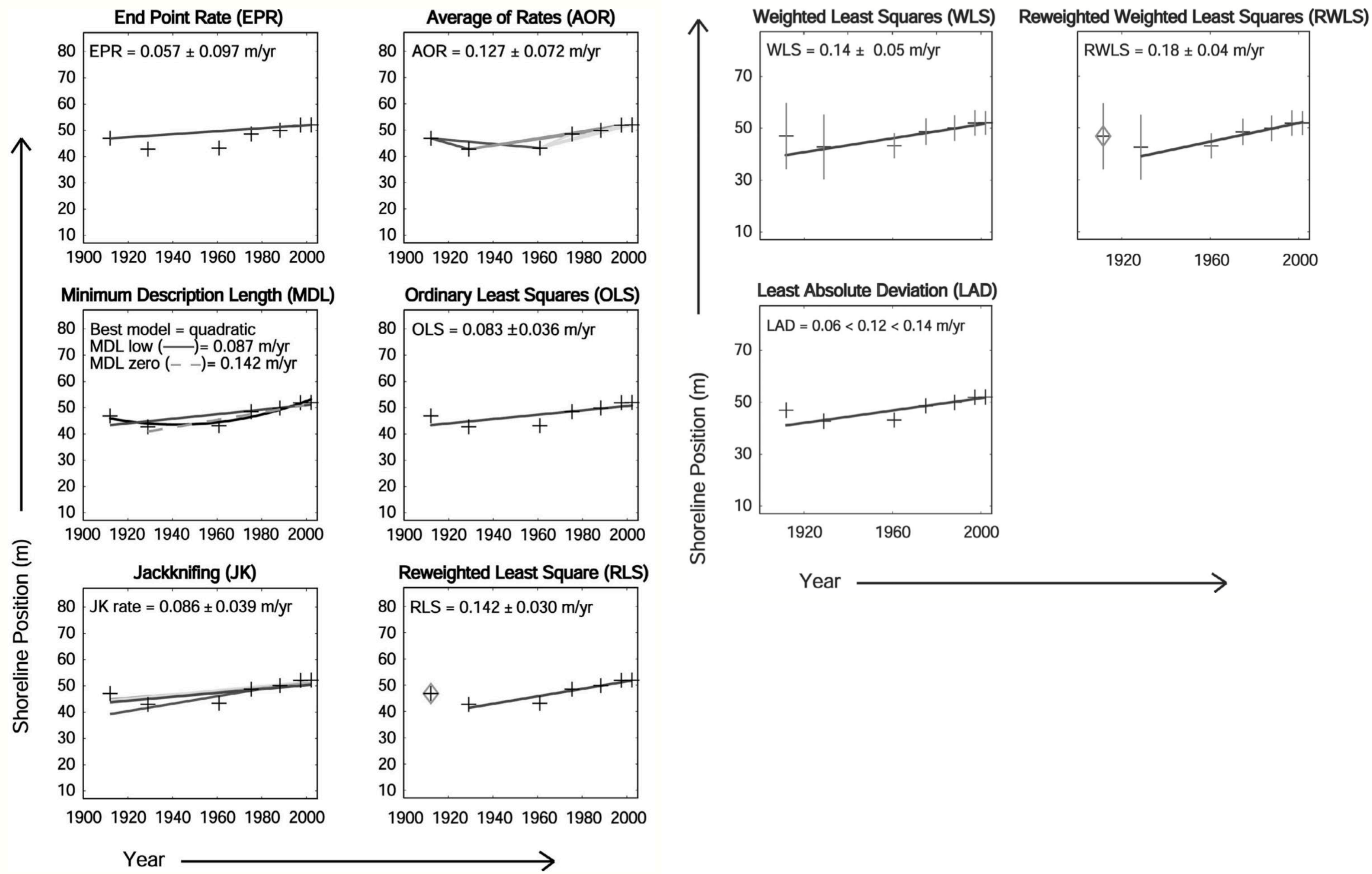

Figure 10. Comparison of rate change statistic methods using shoreline position data (Genz et al. 2007). The EPR, OLS, and WLS are calculated by DSAS with the latter two referred to as LRR and WLR respectively.

Shoreline positions can be calculated from either a transect from baseline method or change polygon method. The change polygon method overlays two shoreline vectors from different years and creates polygons from where the shorelines intersect. These polygons represent erosion or accretion and are added together to get the total area of change. When multiple shorelines are analyzed, change rates for each shoreline are calculated in relation to a baseline. These rates can then be plotted with a regression line to determine the overall rate change (Smith and Cromley 2012).

Transect from baseline methods involve creating transects perpendicular to a baseline and calculating change rates from where the shorelines intersect the transects. Different change rate statistics can then be calculated using two or more of the shorelines. DSAS uses the transect from baseline method and is used in this study. DSAS calculates multiple change rate statistics including EPR, LRR, WLR for each transect (Hemmelstoss, 2018).

Albuquerque et al. (2013) compared the end point rate generated by DSAS and the change polygon method. They used satellite imagery and aerial photographs from 2007 to 2011 to extract shoreline vectors. The resulting statistics from DSAS and the change polygon method linear regression rates were 12.31 m/yr with an R^2 of 13% and 1.76 m/yr with an R^2 of 94% respectively. They concluded that the linear regression rate DSAS reports reflects seasonal variability instead of permanent erosion and accretion. Additionally, Smith and Cromley (2012) found that different rates would be calculated depending on the shoreline morphology and where the baseline is placed. The advantage to DSAS compared to the change polygon method is that proxy-based and datum-based shorelines can be used in the same analysis and rates are calculated for every transect. This means that a greater selection of data over a larger time period can be used.

Chapter 3 Methodology

This chapter discusses the data and methodology for shoreline change analysis used in this study. The DSAS ArcMap add-on is used to calculate change rates from shoreline positions that were extracted from LiDAR derived DEMs and NAIP imagery.

3.1. Data Acquisition and Shoreline Digitization

Shoreline positions are digitized from LiDAR derived DEMs and NAIP imagery, and are the main inputs used in DSAS to calculate shoreline change rates. This study uses both MHW and HWL proxies for shoreline position. The source, date, resolution, and shoreline proxy used for each data set is provided in Table 1. The MHW level calculated for South Beach, Oregon was used for the LLC's MHW value as this is the closest water gauge to the study area, roughly 15 miles south of the study area, and was downloaded from NOAA's Tides & Currents website (NOAA 2021f). For the current epoch, the MHW at South Beach, Oregon is 2.097 m relative to the North American Vertical Datum of 1988 (NAVD88).

A shapefile containing the location, permit, and number of repairs of SPSs along Oregon's coast was retrieved through Oregon's ArcGIS data server (Oregon Parks and Recreation Department 2021). The shapefile was originally created by the Oregon Coastal Management Program to assess the policies regarding SPSs. The database is now managed and updated by Oregon Parks and Recreation Department.

Table 1. The date, source, resolution, and shoreline proxy of the data used in this study.

Dates	Sources	Resolution (m)	Shoreline Proxy
October 17, 1997	NASA/NOAA/USGS	1	MHW
April 27, 1998	NASA/NOAA/USGS	1	MHW
September 9, 2002	NASA/USGS	1	MHW
June 23, 2009	NAIP	1	HWL
2010	U.S. Army Corps of Engineers (USACE)	1	-
June 15, 2012	NAIP	1	HWL
July 1, 2014	NAIP	1	HWL
August 20, 2014	U.S. Army Corps of Engineers (USACE)	1	MHW
April 28, 2016	USGS	0.5	MHW
June 25, 2016	NAIP	1	-

3.1.1. LiDAR Derived DEMs

LiDAR datasets for the Oregon coast are available for download from NOAA's Data Access Viewer (NOAA 2021b). Each dataset has been turned into a digital elevation model (DEM) by the source and is available as a TIFF file. All DEMs were downloaded with the NAD 1983 StatePlane Oregon North horizontal and NAVD88 vertical coordinate systems with both vertical and linear units in feet. The various sources for each dataset are outlined in Table 1. The TIFF files were downloaded as compressed files and were extracted using 7-ZIP file manager (7-zip.org). Shorelines were extracted from the DEMs following similar methodologies to Harris et al. 2006 and Farris et al. 2018. The 2010 DEM data was not utilized in this study because it did not have enough spatial coverage to accurately represent the shoreline throughout the study area.

A polyline representing the shoreline position for each dataset was created by using the Create Contour tool in ArcGIS Pro. The MHW level was used for the baseline with a contour interval of 100 m and a z factor of 1. These polylines were edited to remove line segments that did not represent the shoreline. The shorelines were then smoothed using the Smooth Line tool with the PEAK algorithm and a 10 m tolerance in ArcGIS Pro (Farris et al. 2018).

3.1.2. NAIP Imagery

NAIP imagery was downloaded through USGS's Earth Explorer as compressed TIFF files (USGS 2021). For every year available four images were downloaded to cover the study area. NAIP image specifications are outlined in Table 1. The 7-Zip file manager was again used to extract the compressed files. The TIFFs were imported into TerrSet and converted to IDRISI raster files (.rst) which separated the files into the four spectral bands (red, green, blue, and NIR). The Mosaic tool with average overlap was used to combine the different images into one. A mosaic was created of the green and NIR bands for each year. The normalized difference water index (NDWI) was calculated using Equation (1) and the Overlay tool. NDWI was applied to increase the values of reflected green wavelengths from the surface of the water while decreasing the reflected values of NIR wavelengths (McFeeters 1996). The NDWI images were then exported to TIFF files.

$$NDWI = \frac{Green - NIR}{Green + NIR} \tag{1}$$

In ArcGIS Pro, the NDWI NAIP images were added to the working file geodatabase. The raster images were then reclassified into two classes to identify each pixel as representing either water or land. A threshold value was applied to better represent the HWL, the boundary between visibly wet and dry sand. The threshold value was determined by visually comparing the reclassed image to the color composite image. Due to differences in lighting at the time the image was captured, each year required a different threshold value. The 2016 NAIP imagery was ultimately not used in this study, this is discussed in further detail in Chapter 4. Reclassifying the raster image also converts the raster data to an integer dataset which is required to convert it from a raster to a vector dataset. The vector dataset is composed of polylines that depict the boundaries between the two classes. The polylines are then edited to only include lines representing the HWL.

3.2. **Calculating Shoreline Bias and Uncertainties**

There are uncertainties associated with the accuracy of how data are collected and processed. These uncertainties vary with every step from the collection of LiDAR and aerial imagery to georeferencing and processing, as well as natural variations caused by tide level, waves, and beach slope due to seasonal sediment transport. The uncertainties for each measurement are calculated and are used by the DSAS program to calculate the errors and uncertainties for shoreline change rate statistics. The uncertainties are also used by DSAS when both MHW and HWL shorelines are used in the same shoreline position change calculations.

3.2.1. Proxy-Datum Bias

The offset between MHW and HWL shorelines can vary greatly depending on the slope of the beach and wave runup. Ruggiero and List (2009) determined that this difference between the HWL and MHW positions can be calculated using the tide level (Z_T), MHW level (Z_{MHW}), beach slope ($\tan\beta$), offshore significant wave height (H_o), and offshore wavelength (L_o) in Equation (2). The offshore wavelength can be calculated using linear theory (Equation 3), where g is the acceleration due to gravity and T is the offshore dominant wave period. Ruggiero and

List (2009) determined that if we assume that the HWLs are formed from MHW the offset between the two essentially cancel each other out and give us Equation (4). Average offshore wavelength and wave heights were calculated by NOAA's National Data Buoy Center (NDBC) using data collected by buoy 46050, which is 20 nautical miles offshore of Newport, Oregon (NOAA 2021e).

$$Bias = (X_{HWL} - X_{MHW}) = \frac{\left[Z_T + 1.1(0.35\tan\beta(H_o L_o)^{(1/2)} + \frac{[H_o L_o(0.563\tan\beta^2 + 0.004)]^{1/2}}{2}\right] - Z_{MHW}}{\tan\beta} \quad (2)$$

$$L_o = \left(\frac{g}{2\pi}\right) T^2 \quad (3)$$

$$Bias = (X_{HWL} - X_{MHW}) = \frac{1.1(0.35\tan\ \beta(H_o L_o)^{(1/2)} + \frac{\left[H_o L_o(0.563\tan\beta^2 + 0.004)\right]^{1/2}}{2}}{\tan\beta} \quad (4)$$

3.2.2. HWL Shoreline Uncertainty

Uncertainties associated with the digitization of HWL shorelines from NAIP images are determined by two components. The first is the uncertainty of the accuracy of georeferencing the images (U_g). Starting in 2009, NAIP imagery had to adhere to an "absolute accuracy specification" which requires all georeferenced points to be within 6 m of true ground with a 95% confidence level (U.S. Department of Agriculture 2017). The second uncertainty is the uncertainty of the HWL position when the images were taken (U_{pd}). This is the same calculation as the proxy-datum bias in Equation (4) (Ruggiero et al. 2012). The total uncertainty in HWL shoreline positions (U_{HWL}) are then calculated using:

$$U_{HWL} = \sqrt{{U_g}^2 + {U_{pd}}^2} \tag{5}$$

3.2.3. MHW Shoreline Uncertainty

As with the HWL shoreline uncertainty, the MHW shoreline uncertainty is calculated using two sources associated with data collection. The first uncertainty is the reported horizontal accuracies for each LiDAR derived DEM (U_l). The second uncertainty is the variance of foreshore slope values (U_s). The MHW shoreline position uncertainty (U_{MWL}) is calculated using:

$$U_{MWL} = \sqrt{{U_l}^2 + {U_s}^2} \tag{6}$$

3.2.4. Proxy-Datum Bias Uncertainties

The terms used to calculate the proxy-datum bias, significant wave height, dominant wave period, foreshore beach slope, and water level, have corresponding uncertainties. Ruggiero and List (2009) have derived four equations to compute the proxy-datum bias uncertainty using the above mentioned terms, as follows:

$$\frac{\partial Bias}{\partial Z_T} = \frac{1}{\tan\beta} \tag{7}$$

$$\frac{\partial Bias}{\partial \tan\beta} = \frac{0.31}{[H_0L_0(0.56\tan^2\beta + 0.004)]^{1/2}H_0L_0} + \frac{-Z_T - 0.55[H_0L_0(0.56\tan^2\beta + 0.004)]^{1/2} - Z_{MHW}}{\tan^2\beta} \tag{8}$$

$$\frac{\partial Bias}{\partial H_0} = \left[\frac{0.19\ \tan\beta}{(H_0L_0)^{1/2}}\ L_0 + \frac{0.28}{H_0L_0(0.56\tan^2\beta + 0.004)}\right]^{1/2} \times \frac{L_0(56\ \tan^2\beta + 0.004)}{\tan\beta} \tag{9}$$

$$\frac{\partial Bias}{\partial L_0} = \left[\frac{0.19\ \tan\beta}{(H_0L_0)^{1/2}}\ H_0 + \frac{0.28}{H_0L_0(0.56\tan^2\beta + 0.004)}\right]^{1/2} \times \frac{H_0(56\ \tan^2\beta + 0.004)}{\tan\beta} \tag{10}$$

The uncertainties of each term, δ_H, δ_L, $\delta_{\tan\beta}$, and δ_{Zt}, are calculated following the methods used by Ruggiero et al. (2012). Wave height, wavelength, and beach slope uncertainties are calculated by finding the difference between the 95- and 50-percent exceedance statistics for each term. The assumption that the HWL is at the same elevation as MHW and generated from a previous high tide has the uncertainty of not knowing the water level that left the HWL. This uncertainty is calculated by subtracting MHW from mean higher high water (MHHW). These uncertainties and the derived uncertainty Equations (7- 10) are used in Equation (11) below to calculate the overall proxy-datum bias uncertainty.

$$\delta_{Bias} = \left[\left(\frac{\partial Bias}{\partial Z_T}\delta Z_T\right)^2 + \left(\frac{\partial Bias}{\partial \tan\beta}\delta\tan\beta\right)^2 + \left(\frac{\partial Bias}{\partial H_0}\delta H_0\right)^2 + \left(\frac{\partial Bias}{\partial L_0}\delta L_0\right)^2\right] \tag{11}$$

3.3. **Digital Shoreline Analysis System (DSAS)**

DSAS is an add-on tool in ArcMAP created by USGS to determine the rate of shoreline change. DSAS requires all input data to be stored in a personal geodatabase. At least two digitized shorelines and a user defined baseline are required to calculate shoreline change statistics. DSAS uses the baseline to create perpendicular transect lines that are used in the shoreline change calculations. The DSAS workflow is outlined in Figure 11.

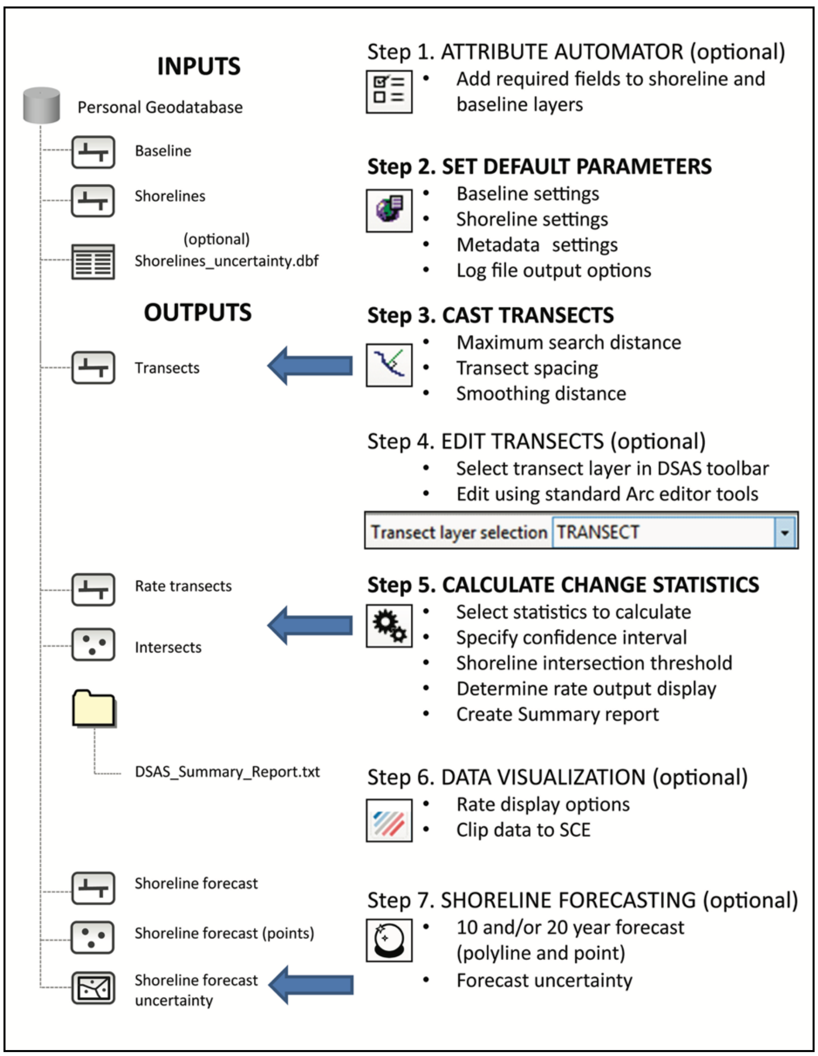

Figure 11. DSAS workflow from the DSAS User Guide (Himmelstoss et al. 2018). Step 7, shoreline forecasting, was not used in this study.

3.3.1. Baseline, Shorelines, and Transects

The DSAS user guide (Himmelstoss et al. 2018) recommends creating a baseline by adding a new feature class to manually draw a line or use a buffer of an existing shoreline. For this project, a buffer 80 m to the left of the 2016 DEM shoreline is used as the baseline. The required attribute fields for the baseline are given in Table 2. The ID field identifies segments of the baseline in order from the beginning to the end of the line. DSAS uses this field to place transect lines in sequence if the baseline is segmented.

Table 2. DSAS baseline geodatabase field requirements (Himmelstoss et al. 2018).

Field Name	Data Type	Attribute addition	DSAS Requirement
OBJECTID	Object identifier	Autogenerated	Required
SHAPE	Geometry	Autogenerated	Required
SHAPE_Length	Double	Autogenerated	Required
ID	Long Integer	User-Created	Required

As required by DSAS, digitized shorelines were merged into a single feature class. A DSAS_date field with the date the LiDAR and NAIP imagery were captured was added to the attribute table as an identifier for each shoreline before the merge. The date field is required by DSAS, the other required fields for the shoreline feature class are given in Table 3. The DSAS_uncy is the shoreline position uncertainty. This is calculated using Equation (5) and (6) for NAIP and DEM derived shoreline positions, respectively. The DSAS_type identifies the specific shoreline as either MHW or HWL. This field is optional and is only used when the two different shoreline proxies are used in the same change rate analysis.

Table 3. DSAS shoreline geodatabase field requirements (Himmelstoss et al. 2018).

Field Name	Data Type	Attribute Addition	DSAS Requirement
OBJECTID	Object identifier	Autogenerated	Required
SHAPE	Geometry	Autogenerated	Required
SHAPE_Length	Double	Autogenerated	Required
DATE_(DSAS_date)	Text (Length=10 OR Length20)	User-Created	Required
UNCERTAINTY (DSAS_uncy)	Any numeric field	User-Created	Required
SHORELINE_TYPE (DSAS_Type)	Text	User-Created	Optional

Transects are automatically drawn by DSAS perpendicular to the baseline. Transect spacing and length can be specified by the user. A transect spacing of 50 m was specified with the option to clip transects at the furthest shoreline extent for this project. After the transects were cast, they were manually inspected and edited to make sure they crossed all the shorelines only once.

3.3.2. Complex Shoreline Data

DSAS allows for both MHW and HWL proxy shorelines to be used in the same shoreline change analysis. To do this, DSAS uses a user defined proxy-datum bias correction (Equation 4) to correct for the difference between the MHW and HWL shorelines. To be able to use both shoreline proxy types, the MHW shorelines need to be converted into a calibrated route, which adds an M-value to each vertex. The M-values are edited to have unique numbers that identify their locations along the shoreline. This ID links the vertices along the MHW shoreline to the proxy-datum bias table. This table contains the information DSAS uses for the proxy-datum bias correction and associated uncertainty calculations, required fields are given in Table 4. The UNCY field is the MHW shoreline uncertainty (U_{MHW}) at each point calculated from Equation (6). The bias field is the proxy-datum bias using Equation (4), and the UNCYB is the uncertainty in the proxy-datum bias from Equation (11).

Table 4. DSAS proxy-datum bias table field requirements (Himmelstoss et al. 2018)

Field Name	Data Type	Field Description
ID	Long Integer	Cross-shoreline LiDAR profile identifier stored as the M-value at each vertex in the calibrated shoreline route. This links the LiDAR shoreline with the uncertainty table.
UNCY	Any numeric field	Positional uncertainty associated with natural influences over the shoreline position (wind, waves, tides) as well as measurement uncertainties associated with the collection of the LiDAR data.
BIAS	Any numeric field	Proxy-datum bias value describing the unidirectional horizontal offset between the MHW elevation of the LiDAR data and the HWL shoreline position.
UNCYB	Any numeric field	Uncertainty of the proxy-datum bas value.

3.3.3. Shoreline Change Statistics

The five statistical values calculated through DSAS are: (1) NSM; (2) SCE; (3) EPR; (4) LRR; and (5) WLR. These statistics are calculated for every transect with rates reported in meters per year. NSM returns the distance in meters between the oldest and youngest shorelines. SCE is the distance in meters between the two furthest shorelines independent of time. The EPR calculates the net shoreline movement rate by dividing NSM by the elapsed time between the oldest and youngest shorelines. Both NSM and EPR only look at the oldest and youngest shorelines and do not take into account any other shorelines.

LRR is calculated by plotting the distance of the shorelines from the baseline against time. A least-squares regression line is fitted to the data, the slope of this line is the shoreline change rate. Like LRR, WLR is calculated using a best fit line. With WLR, the shoreline points are given weights based on their position uncertainty. Points with a smaller uncertainty have a higher weight than those with large uncertainty when determining the placement of the best fit line. Unlike EPR, LRR and WLR use every data point to determine shoreline change rate. Users can specify a confidence level that DSAS uses to calculate the uncertainty of the LRR and WLR. DSAS also calculates the R^2 statistic, for both LRR and WLR, that represents how well the best fit line represents all of the data points (Himmelstoss et al. 2018).

Chapter 4 Results

Chapter 4 provides the results from the outlined methods in Chapter 3 for shoreline digitization and shoreline change analysis through DSAS, using proxy- and datum-based shorelines.

4.1. Shoreline Digitization

Shorelines created from the LiDAR derived DEMs were fairly simple and did not need much editing. When the contour lines were generated, contour lines were also placed where the DEM layer ended. These lines were edited to be removed as they did not represent the shoreline.

The shorelines created from the NAIP imagery were initially a lot messier due to classifying the pixels using NDWI. The polylines generated from the NDWI classified images went through extensive editing to make sure they represented the HWL. Although a threshold was used to help better classify the pixels, many pixels were mis-classified. Pixels containing areas of shadows or roads were classified as water. Figure 12 shows where shadows interfered with the detection of the HWL.

Another factor that influenced the effectiveness of the NDWI classification was the tide level at the time the image was taken. The 2016 NAIP imagery was taken at high tide where the HWL was not discernable. These images were ultimately not used as the NDWI classification did not accurately represent the HWL. Figure 13 shows a section of 2016 NAIP imagery compared with the NDWI classification applied with a 0.09 and 0.1 threshold. The shoreline could have been extracted from the imagery using an alternative method but this was beyond the scope of this project.

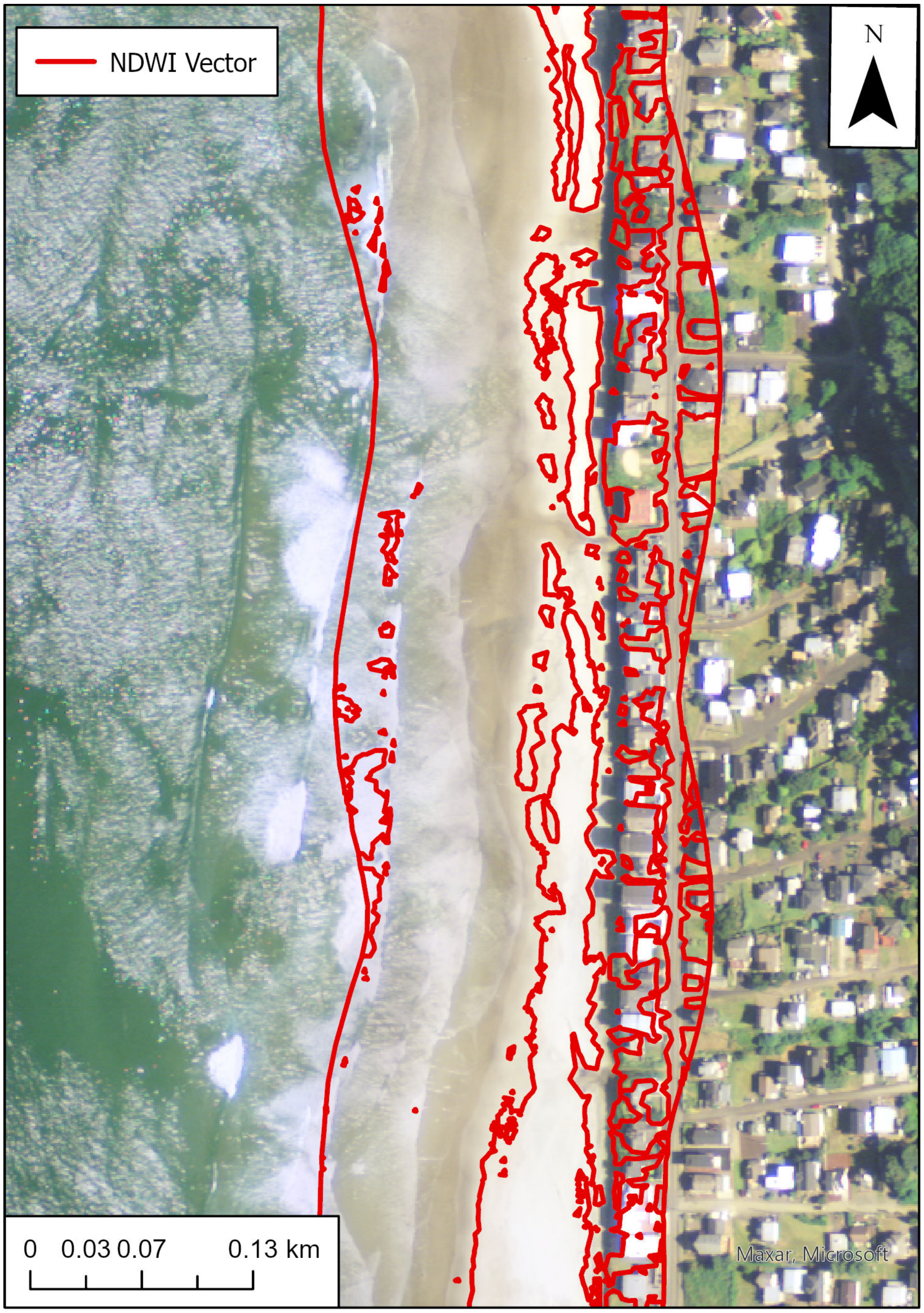

Figure 12. Lines generated from NAIP imagery with NDWI classification showing where shadows and wave swash are mis-classified.

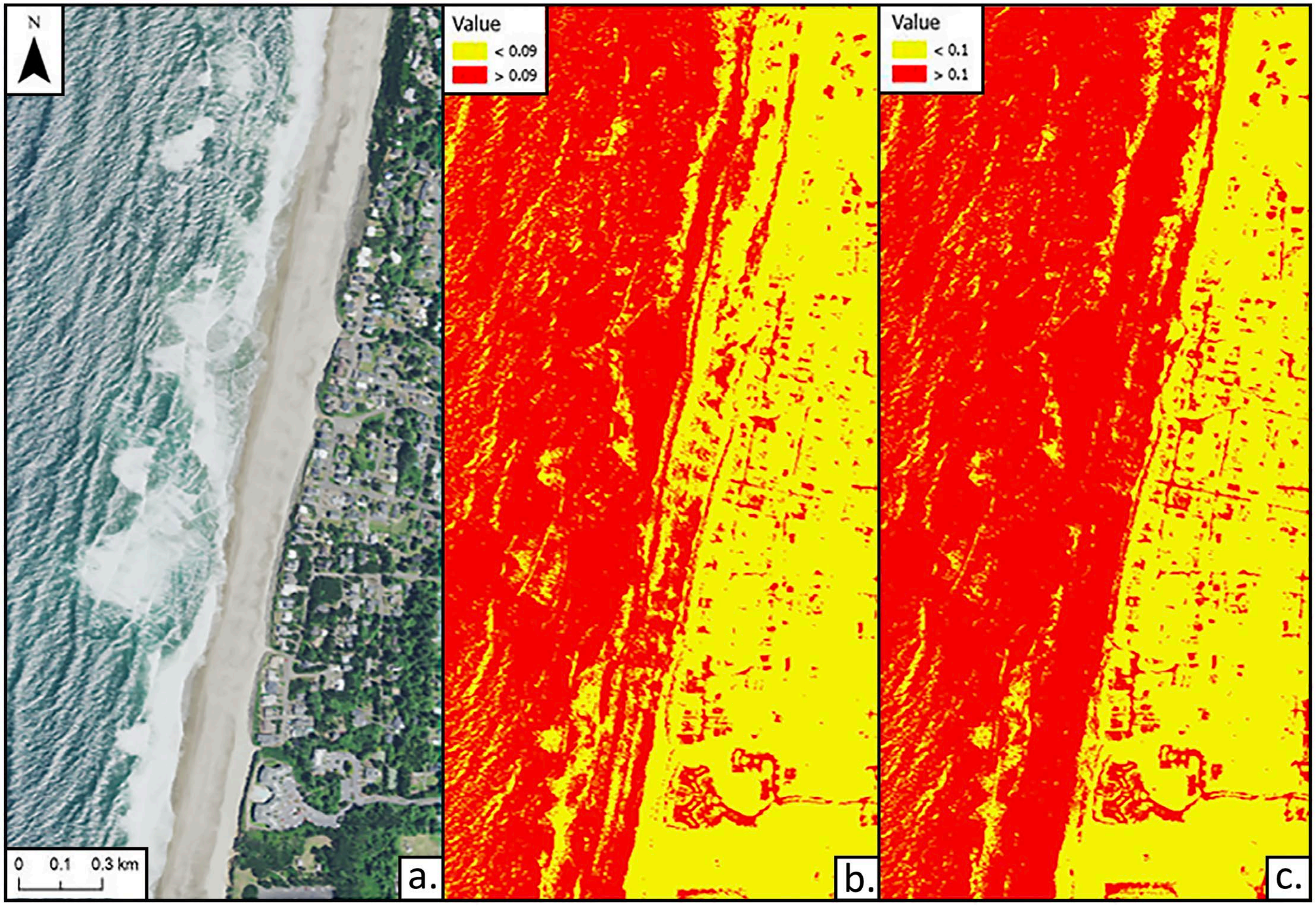

Figure 13. 2016 NAIP imagery (a) and NAIP imagery with NDWI classification applied with a 0.09 threshold (b) and 0.1 threshold (c).

4.2. **Shoreline Change**

After running the shoreline change analysis statistics, DSAS generates two new feature classes. The first new feature class is a copy of the transect feature class with the addition of shoreline change statistics. The second contains points that hold position records where the transect lines cross the shorelines. In addition to these feature classes, a text document is generated containing a summary report that provides the averages for each of the calculated statistics.

4.2.1. Overall Shoreline Change

DSAS statistics were generated for two periods, 1997-2016 and 1997-2014. The shoreline for 2016 was generated using LiDAR data collected on April 28, 2016. The period from roughly July 2015 through April 2016 was considered a very strong El Niño (see Figure 3). Powerful waves generated by large storm systems during El Niño events influence shoreline position. Because of this, the DSAS statistics were run for the shorelines from 1997 to 2014 to remove any variations that might have been caused by these larger than average storm surges.

The average shoreline change rates along with percent erosion and accretion from the DSAS summary report are given for both the 1997-2016 and 1997-2014 shoreline date groups in Table 5. The full summary reports for both date groups are provided in Appendix A and Appendix B.

The shoreline change analysis for 1997-2016 shows that overall, there is a general trend of accretion within the LLC. The average NSM between 1997 and 2016 is 5.18 m with an average EPR of 0.32 m/yr. The average LRR is 1.21 m/yr while the average WRR is 1.06 m/yr.

Although the average shoreline rate shows that accretion is the dominant trend, there are sections of the shoreline that are eroding.

Table 5. The average shoreline changes rates and percent erosion and accretion for each statistic from the DSAS summary report for shorelines between 1997-2016 and 1997-2014.

Date Group		SCE (m)	NSM (m)	EPR (m/yr)	LRR (m/yr)	WLR (m/yr)
1997-2016	Average	78.88	5.18	0.32 +/- 0.58	1.21 +/- 0.58	1.06 +/- 0.6
	Percent erosion	-	42.82%	42.82%	29.17%	28.94%
	Percent accretion	-	57.18%	57.18%	70.83%	71.06%
	Maximum erosion	-	-57.67	-3.55	-3.15	-3.07
	Maximum accretion	-	168.47	12.38	10.57	10.21
1997-2014	Average	76.74	19.71	1.2 +/-0.6	1.86 +/- 0.7	1.42 +/- 0.73
	Percent erosion	-	24.94%	22.76%	22.76%	25.91%
	Percent accretion	-	75.06%	75.06%	77.24%	74.09%
	Maximum erosion	-	-43.49	-2.7	-2.94	-2.84
	Maximum accretion	-	202.59	12.03	16.91	14.13

The EPR calculates the position change from the youngest shoreline to the oldest, whereas the WLR plots all shoreline positions giving the points with smaller uncertainty values more weight and uses the slope of a best fit line to calculate the rate of change. The change rate value calculated by EPR and WLR are notably different, 0.32 m/yr and 1.06 m/yr respectively for 1997-2016. The differences between these two rate calculations are compared in Figure 14. Figures 15 and 16 compare the EPR and WLR rate graphs spatially to the shoreline. The WLR rates show that the northern section of the shoreline is accreting at a faster rate than when calculated by the EPR.

Like the 1997-2016 shoreline change rates, the 1997-2014 change rates show that there was an overall trend of accretion throughout the study area. With the 2016 shoreline removed, the average shoreline rate change increased. The EPR, LRR, and WLR rates differed by 0.88, 0.65, and 0.36 m respectively, while the NSM increased from 5.18 m to 19.71 m. The difference in NSM from the shoreline groups show that the 2016 shoreline was located further inland compared to the 2014 shoreline indicating an erosional period and agreeing with the trend of erosion during El Niño events.

Both shoreline groups show that erosion is more frequent in the southern section of the study area. This follows the general pattern where erosion is more prominent in the southernmost section of the coastline when it is bound on either side by headlands, and that erosion occurs at greater rates during El Niño warm phases.

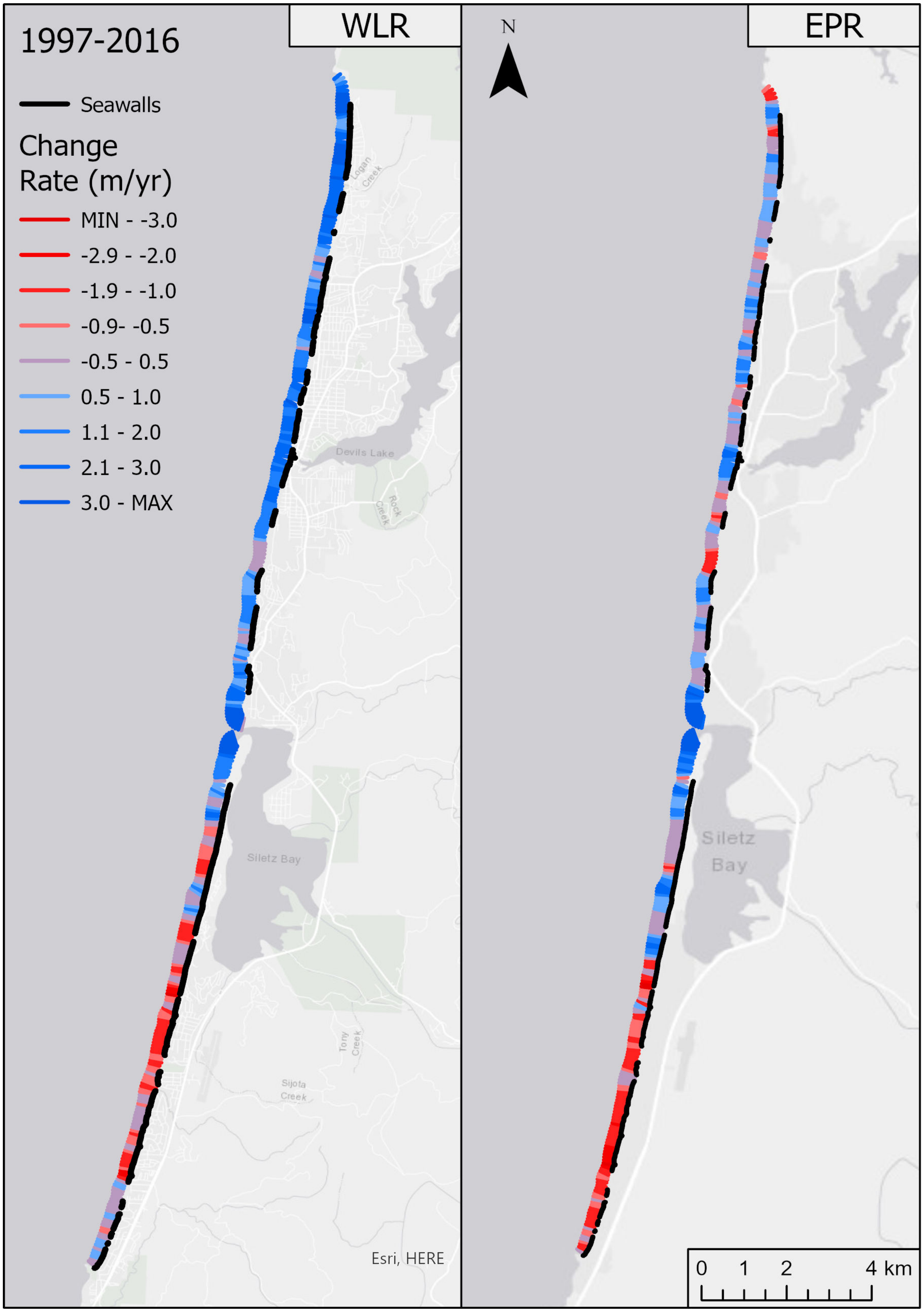

Figure 14. Change rates in meters per year for shorelines between 1997-2016 calculated by WLR (left) and EPR (right).

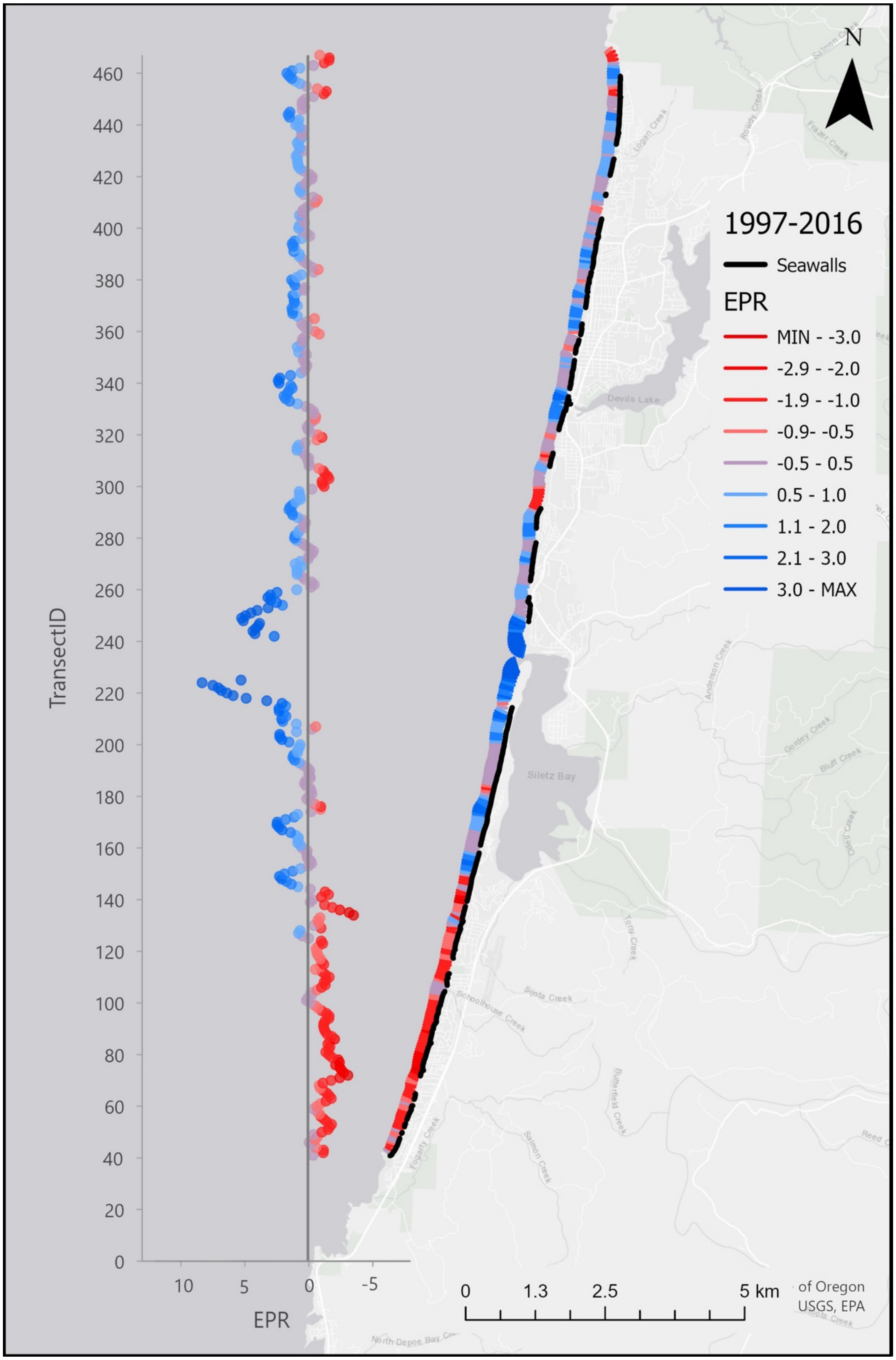

Figure 15. The EPR for the 1997-2016 shorelines.

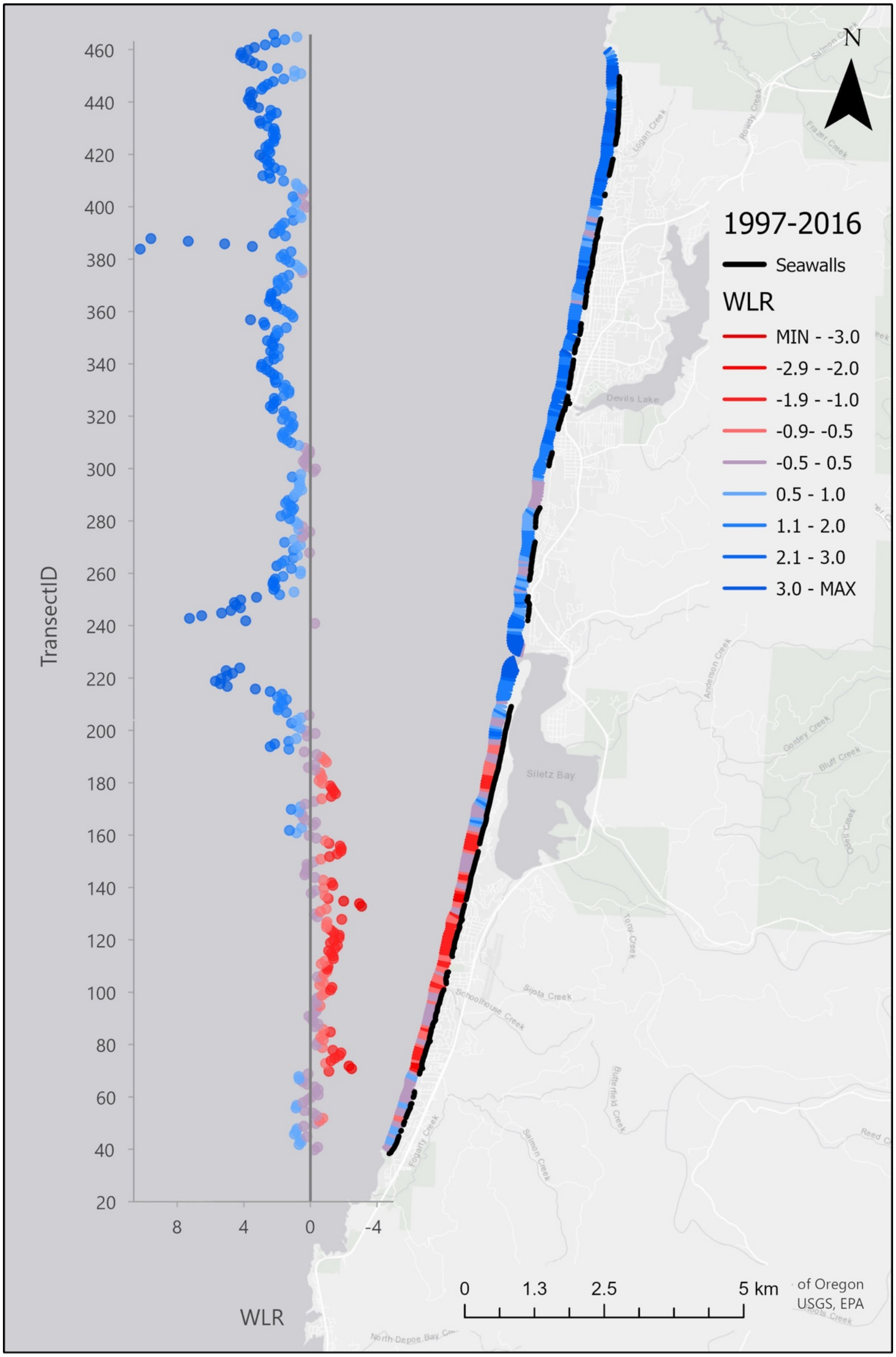

Figure 16. The WLR for the 1997-2016 shorelines.

4.2.2. Shoreline Change with Respect to Seawalls

To better view the shoreline changes with respect to seawall position, the seawalls have been sectioned into 19 groups and numbered from south to north. Figure 17 shows the location of each seawall group and the NSM for both date groups. The NSM for the 1997-2016 shorelines show that there is some correlation between seawall placement and areas of erosion and accretion. The 1997-2014 shorelines show less of a correlation with the majority of erosion occurring between shoreline groups 1 and 5. Table 6 lists the counts of erosion and accretion occurring at the beginning and ends of the seawall groups. From this data, there is no discernible pattern to where erosion and accretion are occurring in relation to seawalls.

Table 6. Count of the occurrence of erosion or accretion at the beginning and end of the seawall groups.

Year Group	Change Rate Statistic	Beginning		End	
		Erosion	Accretion	Erosion	Accretion
1997-2016	EPR	10	9	8	11
	WLR	4	15	5	14
1997-2014	EPR	3	16	5	14
	WLR	8	11	10	9

Shoreline rate change associated with SPSs is most apparent when looking at the EPR for the 1997-2016 shorelines. Figure 18 takes a closer look at the 1997- 2016 EPR. In Figure 18 (c) and (d) shoreline retreat is occurring directly at the ends of all the shoreline groups except 10, 13 and 19. Figure 19 shows the EPR for the 1997- 2014 shorelines, here shoreline change is not occurring at the beginning and ends of the SPSs like in the 1997-2016 change rate map. Figure 19 (c) shows that for the most part, the shoreline is retreating only in front of the SPSs.

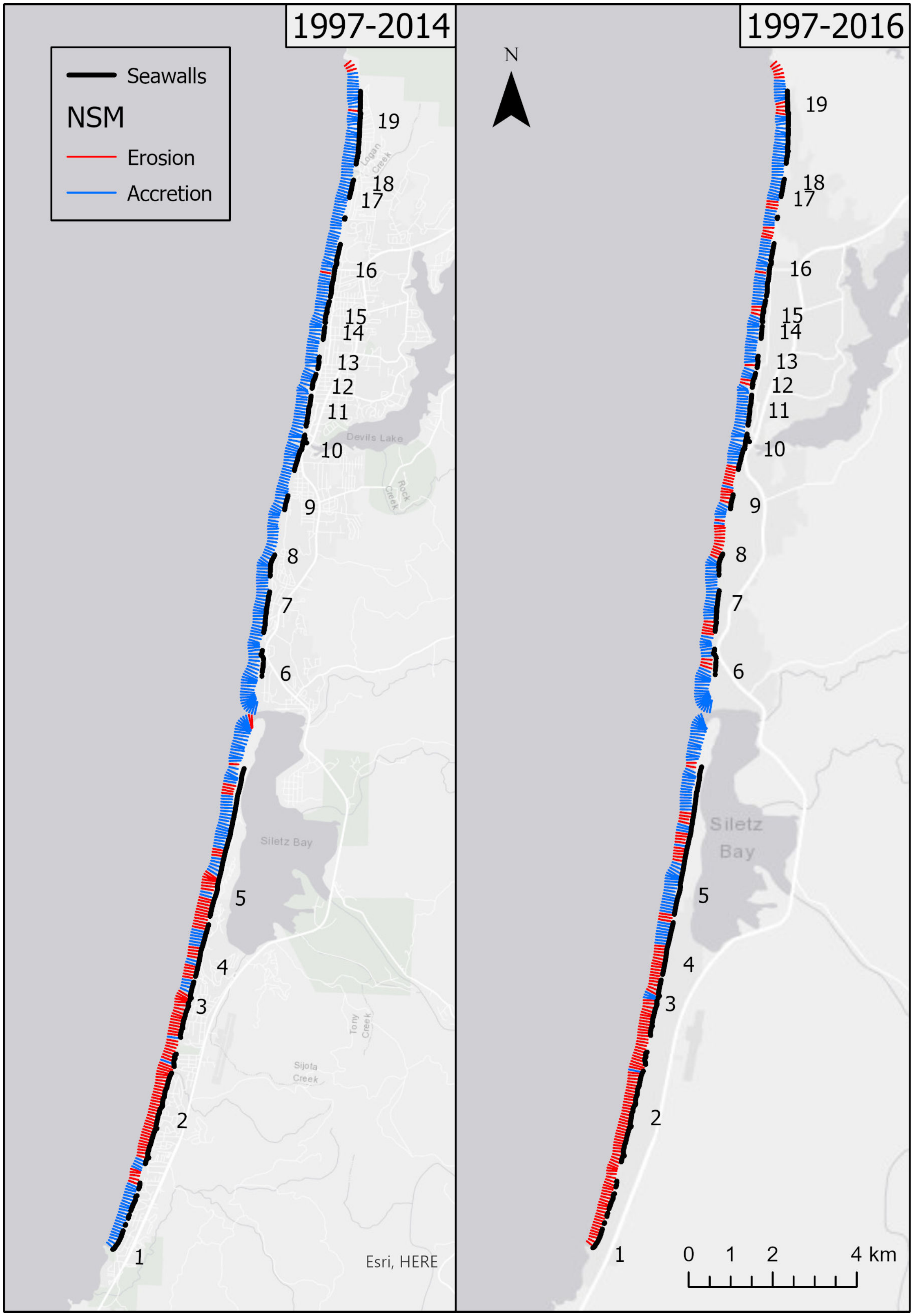

Figure 17. Comparison of NSM in meters from 1997-2014 (left) and 1997-2016 (right).

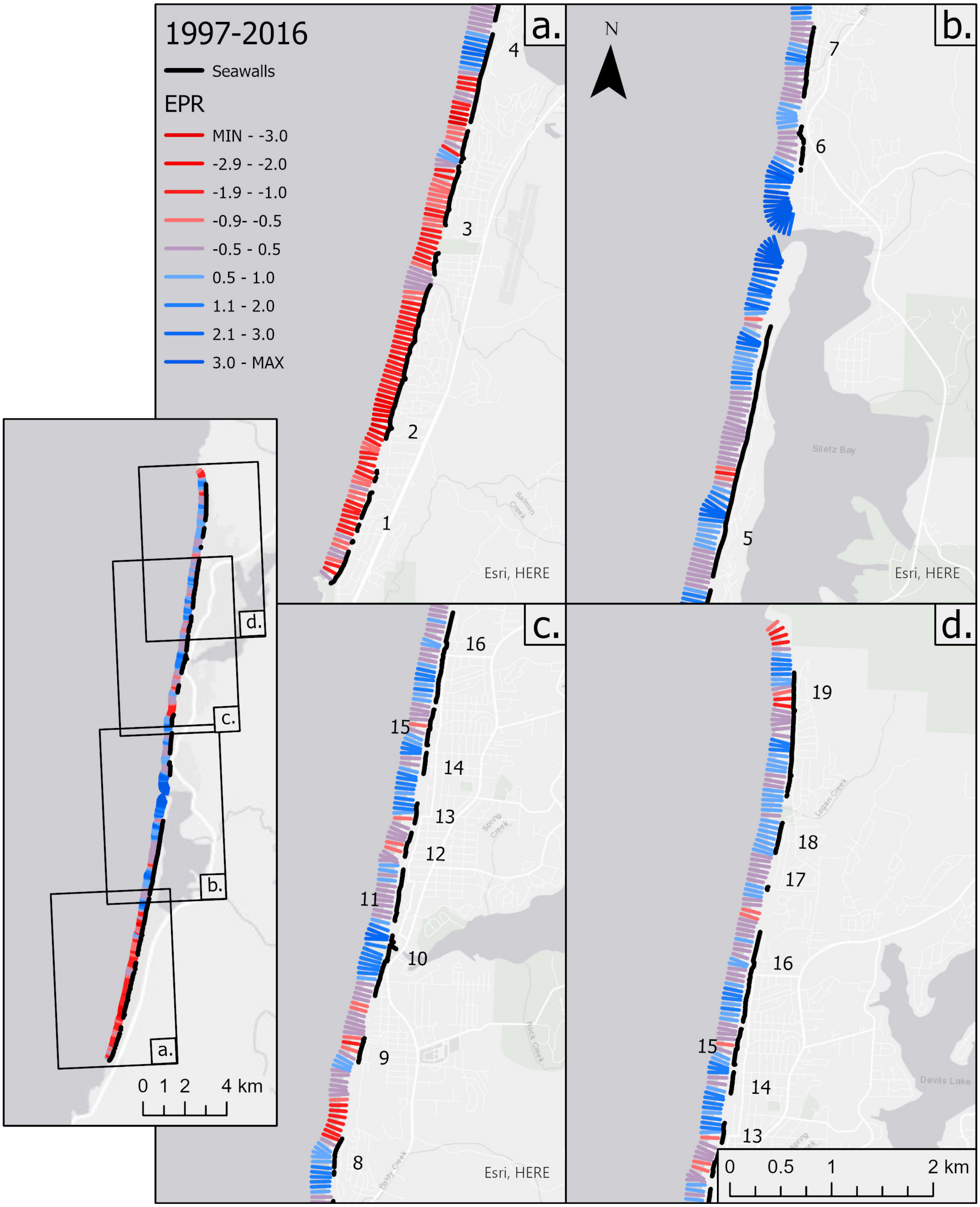

Figure 18. A closer look at the EPR for the 1997-2016 shorelines.

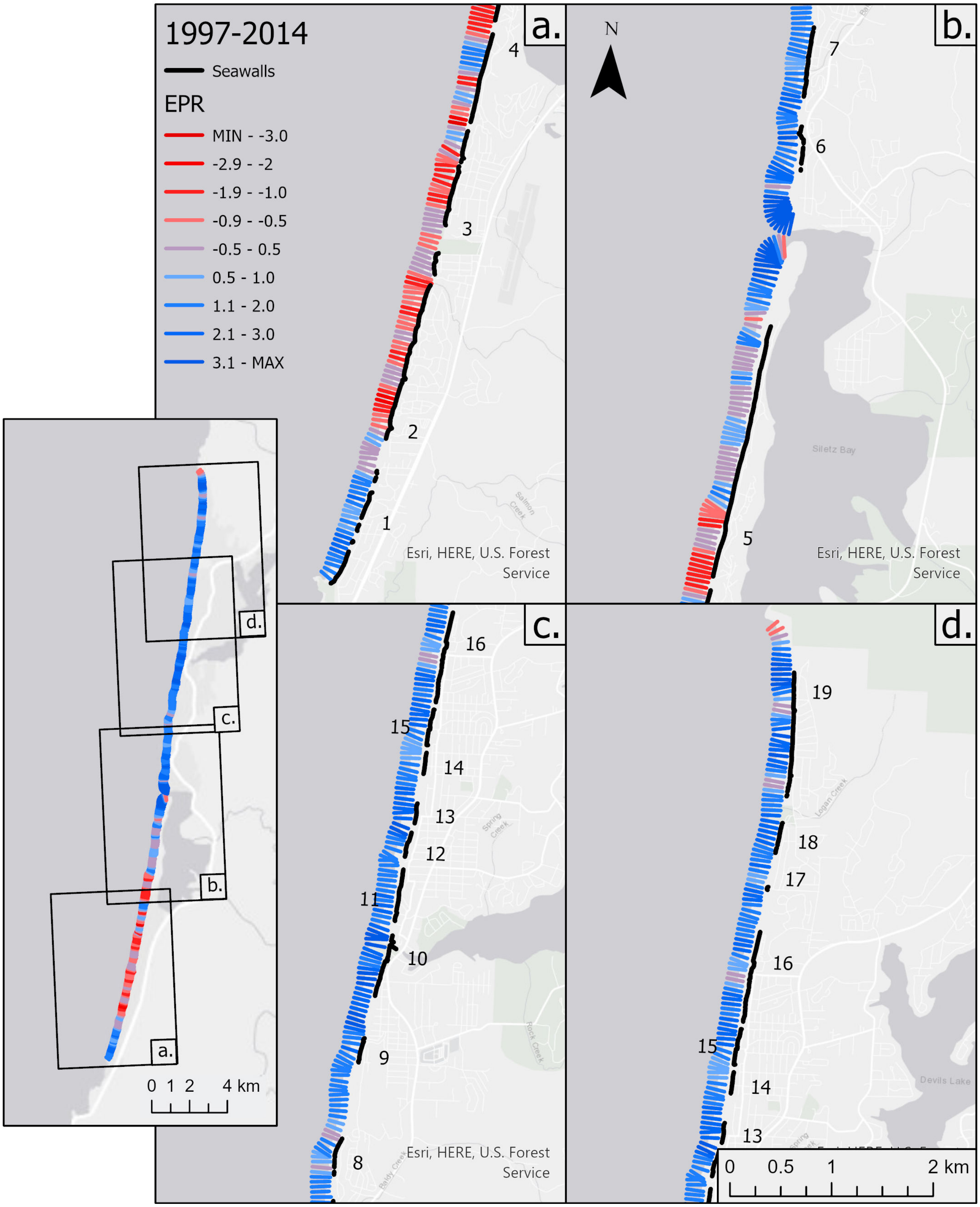

Figure 19. A closer look at the EPR for the 1997-2014 shorelines.

Chapter 5 Discussion and Conclusions

This chapter discusses the findings from the shoreline change analysis as well as the methods used and how these findings and methods can be applied to future research and coastal policy.

5.1. Limitations and Future Improvements

NAIP imagery was chosen for this study due to its spatial and temporal availability, having a 1 m resolution, as well as being free-of-charge to the public. An advantage to NAIP imagery, compared to other aerial imagery, is that a CNIR sensor is used. CNIR sensors capture the red, blue, green, and NIR wavelengths. Because each wavelength is recorded separately, the NDWI was able to be calculated using the green and NIR bands. As discussed in Chapter 2, new indices have been created to improve upon NDWI and better delineate pixels representing water versus land. Some of these indices utilize middle infrared (MIR) wavelengths that are not recorded by the CNIR sensors. Using satellite imagery that captures MIR in conjunction with one of the updated water indices might have provided more accurate results and made shoreline digitization slightly easier. The next available highest spatial resolution and free-of-charge data for the study area was imagery from the Landsat satellites, but due to the 30 m resolution and a mean daily tidal range of 1.9 m along the LLC shore, these images were not used.

The use of NDWI to digitize the shoreline was not optimal for the data and study area used in this study. The placement of the HWL was highly variable based on when the image was taken and the tide level at the time, as shown in Figures 12 and 13. Using a different method, such as manual delineation, might provide more accurate and consistent shoreline placement.

Shoreline change analysis shows erosion and accretion through the seaward or landward movement of the shoreline. Although this provides a good indication of where erosion and accretion are occurring, it does not provide information on how the morphology of the shore is changing. In addition to the methods used in this study, future analysis could use the DEMs to analyze the sediment volume change to better visualize where erosion and accretion are occurring with respect to the SPSs. This could provide more insight into the long-term effects of the structures.

5.2. **Analysis of Shoreline Change Rates**

This study found that overall, the majority of the shoreline is accreting. Depending on the statistical method used, the average change rates range from 0.32 to 1.42 m/yr. These rates vary greatly compared to the short-term change rate calculated by Ruggiero et al. (2013) of -0.3 m/yr. The difference between this study and that of Ruggiero et al. (2013) are the time periods evaluated. Ruggiero et al. (2013) used shorelines from the 1960s to 2002 whereas this study looked at shorelines from 1997 to 2016.

This difference can be explained by the decadal coastal variability described by Anderson et al. (2018). In 2002 the PDO index was at the end of a cool phase. The latest warm PDO phase started in 2014 and peaked in April 2016, which is when the LiDAR data was collected for both the 2014 and 2016 shorelines used in this study. According to Anderson et al. (2018), warm PDO phases are characterized by an increase in wave power along the Oregon coast compared to cool phases. This results in erosion being focused at the southern ends of littoral cells and accretion at the northern ends. This pattern of erosion and accretion is reversed during cool phases and can be seen when the change rates calculated in this study are compared with those of Ruggiero et al. (2013) and the PDO index shown in Figure 20.

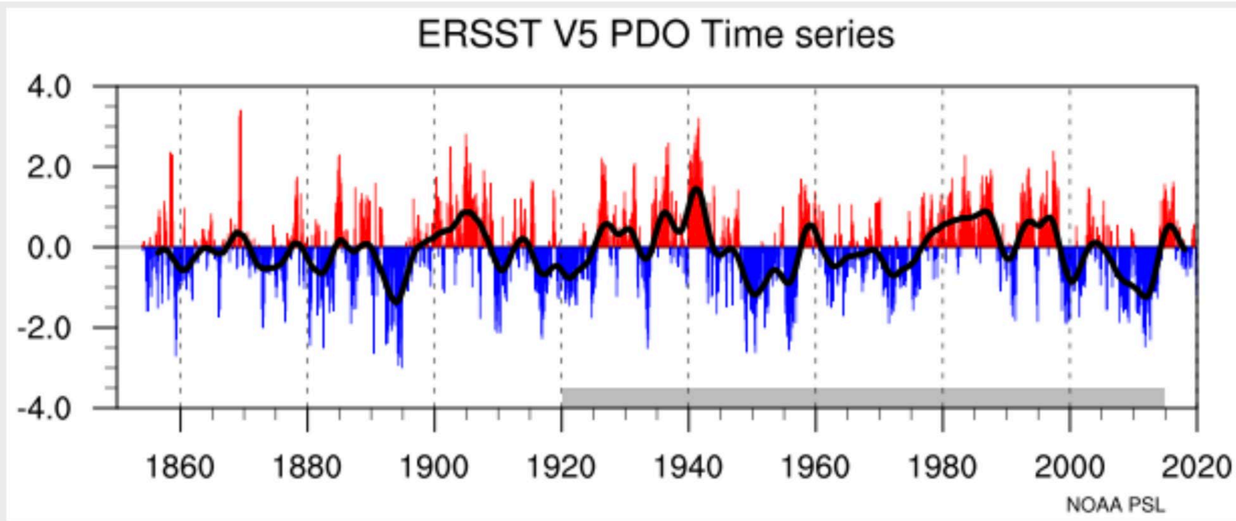

Figure 20. Graph showing the cool and warm phases of the PDO (NOAA 2021d).

As discussed in Chapters 1 and 2, it is known that SPSs can cause disruptions in the natural cycle of sediment transport within a littoral cell. Specifically for seawalls, these disruptions appear as sediment being trapped behind the wall and erosion occurring at the base and ends of the wall. For the 1997-2016 shorelines the end point rate (EPR) showed that 47% of the 19 seawall segments had erosion occurring at either end whereas the weighted linear regression (WLR) showed only 21% had erosion. The EPR and WLR change rates for the 1997-2014 shorelines were opposite with 24% and 42% respectively. Both the EPR and WLR for both shoreline groups indicate that in general, the seawalls within the study area are serving their purpose and protecting structures from shoreline retreat. Although the data show that accretion is the prominent trend throughout the study area, they also highlight areas where erosion is occurring adjacent to seawalls. This is made even more apparent when looking at the DEM subtractions showing the change in elevation around the seawalls.

The difference in the 1997-2016 and 1997-2014 data show that the DSAS rates are influenced by seasonal variability. This seasonal shoreline variability makes it difficult to analyze any long-term effects caused by seawalls. However, by comparing the two date groups and identifying the patterns of seasonal variability, these results demonstrated that shoreline change analysis can be used to identify areas of erosion caused by seawalls. This can be of importance for coastal planners and managers when making decisions, such as setback distances, that consider the variability and effects of 100-year storms.

Both the EPR and WLR change rates were compared in this study. Their calculated rate changes for both date groups differed by 0.74 and 0.22 for 1997-2016 and 1997-2014 respectively. Although Genz et al. (2007) found WLR to be the most accurate statistic to calculate rate changes with uncertainties, both Allen et al. (2003) and Ruggiero et al. (2013) determined that WLR should only be used for long-term studies. This is because WLR assumes a linear trend in shoreline change and can be influenced by outliers like shorelines recently affected by a large storm system. EPR is used for short-term rate changes calculated by Ruggiero et al. (2013) because it only uses the oldest and most recent shorelines and therefor does not assume a linear trend. Seasonal variability is reflected in EPR as shown by the comparison of the 1997-2014 and 1997-2016 change rates in this study. In contrast, the 1997-2016 WLR more closely resembled the 1997-2014 EPR.

5.3. **Coastal Policy**

Currently, Oregon has policies in place to help protect the beach and keep it accessible to the public. Goal 18 is one of these policies that defines where SPSs can be constructed, and the requirements needed for homeowners to acquire a permit to build one. Gardner (2015) assessed these policies and discussed how they could be improved. One of these improvements suggests that policies need to address future climate change and adaptation planning. Goal 18 only specifies that SPSs need a permit if they are to be constructed beyond the vegetation line, which defines the boundary between the state recreation area and private land (DLDC 2021; ORS 2019) To bypass this, homeowners have been building SPSs behind the vegetation line to prepare for future shoreline retreat; once these structures are exposed or collapse, it is the homeowner's responsibility to clean up the debris (Gardner 2015). This is becoming a more common occurrence. In March of this year, an unpermitted seawall collapsed onto the beach leaving three houses exposed to future erosion (Figure 21) (Brock 2021). This property is located at the southernmost end of the LLC where current erosion rates are high. It has been nearly 20 years since the last shift of the PDO. If the 20- to 25-year trend continues, the PDO should enter into a warm phase soon. This implies that there will be an increase in El Niño events and ultimately an increase in erosion, specifically at the southern end of the LLC.

Figure 21. Seawall collapse at the southern end of the LLC leaving three houses dangerously exposed to further cliff (Brock 2021).

Two other improvements to policies Gardner (2015) highlights are specifying the structure design and requiring impact reports of a structure for the entire littoral cell instead of just to adjacent properties. Hard structures, such as seawalls and riprap, are currently the only erosion mitigation efforts in place within the LLC. Gardner (2015) suggests that policy makers look into alternate mitigation efforts such as vegetation stabilization, cobble revetments, and beach nourishment. Once more is known about trends in shoreline variability associated with long-term events, such as the PDO, Stive et al. (2002) proposes that beach nourishment can be placed more effectively and efficiently.

This study shows that future research using similar short-term shoreline change analysis can help by providing the necessary information needed to fill in the gaps of current coastal policies in Oregon. With the correlation between the PDO and shoreline variability, shoreline change analysis can focus on past events that are similar to current or future conditions. This can then be used to improve policy relating to emergency situations like the SPSs collapse this year. By analyzing the entire shoreline within a littoral cell over different periods of time and wave conditions, a better understanding of how SPSs affect the entire littoral cell can be made. Knowing how the shore changes under varying conditions and how SPSs influences this, will lead to improved decision making and safer mitigation efforts.

5.4. **Conclusions**

Identifying the connection between the PDO and shoreline variability along the Oregon Coast is a major step in better understanding coastal processes and how they affect the shore. Most of the studies reviewed in Section 2.2 emphasize that future hazard assessments, policy decisions, and SPSs construction take into consideration the centennial and decadal influences on shoreline variability (Allan and Komar 2006; Barnard et al. 2015; Ruggiero et al 2013; Stive

2002). Future research can build upon studies like this one, that use short-term shoreline change analysis to observe the affects SPSs have on the surrounding shore, to help preserve the coast and coastal communities.

This study found that short-term shoreline change analysis can be used to identify seasonal variability, specifically the variability between an average and El Niño years, and was able to identify variability due to the PDO when compared to previous shoreline change analysis. To improve upon this study and to get a better picture of shoreline variability, EPR analysis should be used to compare shorelines that have been influenced by known factors, such as El Niño or La Niña years. Comparing these could help identify trends in shoreline change directly related the influencing factors and could potentially help identify other factors and trends in shoreline change. Additionally, volumetric change analysis using LiDAR data would be beneficial in the assessment of how SPSs affect shore morphology. Volume change analysis would be able to show where sediment is gained and lost in relation to SPSs, help identify a littoral cell's sediment budget, and trends in sediment transport. There are many unknowns about the processes that influence coastal morphology and how their interactions with SPSs will affect the morphology. Hopefully, the methods and ideas presented in this study can be used to help improve the way SPSs and associated erosion hazards are assessed and addressed.

References

Allan, J. C., Komar, P. D., Priest, G. R. 2003. "Shoreline Variability on the High-Energy Oregon Coast and its Usefulness in Erosion-Hazard Assessments." *Journal of Coastal Research* Special Issue (38): 83-105.

Allan, J. C., Komar, P. D. 2006. "Climate Controls on US West Coast Erosion Processes." *Journal of Coastal Research* 22 (3): 511-529.

Anderson, D., Ruggiero, P., Antolinez, J. A. A., Mendez, F. J., Allan, J. 2018. "A Climate Index Optimized for Longshore Sediment Transport Reveals Interannual and Multidecadal Littoral Cell Rotations." *Journal of Geophysical Research: Earth Surface* 123: 1958-1981.

Barnard, P. L., Short, A. D., Harley, M. D., Splinter, K. D., Vitousek, S., Turner, I. L., Allan, J., et al. 2015. "Coastal Vulnerability Across the Pacific Dominated by El Niño/Southern Oscillation." *Nature Geoscience* 8: 801-808.

Boak, E. H., Turner, I. L. 2005. "Shoreline Definition and Detection: A Review." *Journal of Coastal Research* 21 (4): 688-703.

Brock, M. 2021 "Cliffside homes on Oregon Coast threatened by seawall collapse." Oregon Live. Accessed April 30, 2021. https://www.oregonlive.com/news/2021/03/cliffside-homes-on-oregon-coast-threatened-by-seawall-collapse.html

Cai, W., Borlace, S., Lengaigne, M., van Rensch, P., Collins, M., Vecchi, G., Timmermann, A., et al. 2014. "Increasing Frequency of Extreme El Niño Events Due to Greenhouse Warming." *Nature Climate Change* 4: 111-116.

Cazenave, Anny, and Gonéri Le Cozannet. 2014. "Sea Level Rise and Its Coastal Impacts." *Earth's Future* 2 (2): 15–34.

Darwish, K., Smith, S. E., Torab, M., Monsef, H., Hussein, O. "Geomorphological Changes along the Nile Delta Coastline between 1945 and 2015 Detected Using Satellite Remote Sensing and GIS." *Journal of Coastal Research* 33 (4): 786-794.

Department of Land Conservation and Development Commission (DLDC). 2021. "Oregon's Statewide Planning Goals & Guidelines." 1988. *Goal 18: Beaches and Dunes*. OAR 660-015-0010(3). Accessed April 25, 2021. https://www.oregon.gov/lcd/OP/Documents/goal18.pdf

Farris, A. S., Weber, K. M., Doran, K. S., List, J. H. "Comparing Methods Used by the U.S. Geological Survey Coastal and Marine Geology Program for Deriving Shoreline Position from Lidar Data." U.S. Geological Survey Open-file report 2018-1121, 13p., Feyisa, Gudina L., Henrik Meilby, Rasmus Fensholt, and Simon R. Proud. 2014. "Automated Water Extraction Index: A New Technique for Surface Water Mapping Using Landsat Imagery." *Remote Sensing of Environment* 140 (January): 23–35.

Fisher, Adrian, Neil Flood, and Tim Danaher. 2016. "Comparing Landsat Water Index Methods for Automated Water Classification in Eastern Australia." *Remote Sensing of Environment* 175 (March): 167–82.

Gardner, M. 2015. "Analysis of Shoreline Armoring & Erosion Policies," 64.

Genz, A. S., Fletcher, C. H., Dunn, R. A., Frazer, L. N., Rooney, J. J. 2007. "The Predictive Accuracy of Shoreline Change Rate Methods and Alongshore Beach Variation on Maui, Hawaii." *Journal of Coastal Research* 23 (1): 87-105.

Gill, S. K., Schultz, J. R. 2001. "Tidal Datums and Their Applications." NOAA National Ocean Service Center for Operational Oceanographic Products and Services. 58.

Good, J. W. 1992. "Ocean Shore Protection Policy and Practices in Oregon: An Evaluation of Implementation Success." Doctoral Thesis. Oregon State University.

Harris, M., Brock, J., Nayegandhi, A., Duffy, M. 2006. "Extracting Shorelines from NASA Airborne Topographic Lidar-Derived Digital Elevation Models." U.S. Geological Survey Open-file report 2005-1427.

Hiller, Priska H., Leif Lia, and Jochen Aberle. 2019. "Field and Model Tests of Riprap on Steep Slopes Exposed to Overtopping." *Journal of Applied Water Engineering and Research* 7 (2): 103–17.

Himmelstoss, E.A., Henderson, R.E., Kratzmann, M.G., and Farris, A.S., 2018, Digital Shoreline Analysis System (DSAS) version 5.0 user guide: U.S. Geological Survey Open-File Report 2018–1179, 110 p.,

IPCC. 2013. "Sea Level Change." *Climate Change 2013: The Physical Science Basics. Contribution of Working Group I to the Fifth Assessment Report of the Intergovernmental Panel on Climate Change* 1137-1216.

Kauffman, D. 2018 "Additional Riprap Pictures." Dan Kauffman Excavating, Inc. Accessed May 26, 2021. dan.kauffmanexcavating.com/riprap-more-pics.html.

Kelly, J. T., Gontz, A. M. 2018. "Using GPS-Surveyed Intertidal Zones to Determine the Validity of Shorelines Automatically Mapped by Landsat Water Indices." *International Journal of Applied Earth Observation and Geoinformation* 65 (March): 92–104.

Komar, P. D., Allan, J. C., Ruggiero, P. 2011. "Sea Level Variations along the U.S. Pacific Northwest Coast: Tectonic and Climate Controls." *Journal of Coastal Research* 27 (5): 808-823.

Komar, P. D., Shih, S-M. 1993. "Cliff Erosion along the Oregon Coast: A Tectonic-Sea Level Imprint Plus Local Controls by Beach Processes." *Journal of Coastal Research* 9 (3): 747–65.

Kraus, N. C., McDougal W. G. 1996. "The Effects of Seawalls on the Beach: Part I, An Updated Literature Review." *Journal of Coastal Research* 12 (3): 691–701.

McFeeters, S. K. 1996. "The Use of the Normalized Difference Water Index (NDWI) in the Delineation of Open Water Features." *International Journal of Remote Sensing* 17 (7): 1425–32.

McFeeters, S. K. 2013. "Using the Normalized Difference Water Index (NDWI) Within a Geographic Information System to Detect Swimming Pools for Mosquito Abatement: A Practical Approach." *Remote Sensing* 5 (2013): 3544-59.

Moore, L. J., Ruggiero, P., List, J. H., "Comparing Mean High Water and High Water Line Shorelines: Should Proxy-Datum Offsets Be Incorporated into Shoreline Change Analysis?" *Journal of Coastal Research* 22 (4): 894-905.

Newman, M., Alexander, M. A., Ault, T. R., Cobb, K. M., Deser, C., Di Lorenzo, E., Mantua, N. J. 2016. "The Pacific Decadal Oscillation, Revisited." *Journal of Climate* 29: 4399-4424.

NOAA. 2021a. "Cold & Warm Episodes by Season." National Weather Service Climate Prediction Center. Accessed April 15, 2021. https://origin.cpc.ncep.noaa.gov/products/analysis_monitoring/ensostuff/ONI_v5.php

NOAA. 2021b. "Data Access Viewer." 2021. NOAA. Accessed January 21, 2021. https://coast.noaa.gov/dataviewer/#/LiDAR/search/

NOAA. 2021c. "Economics and Demographics." 2020. Accessed November 8, 2020. https://coast.noaa.gov/states/fast-facts/economics-and-demographics.html.

NOAA. 2021d. "Pacific Decadal Oscillation (PDO)." NOAA Physical Sciences Laboratory. Accessed April 20, 2021. https://psl.noaa.gov/pdo/

NOAA. 2021e. "Station 46050." NOAA National Data Buoy Center. Accessed March 21, 2021. https://www.ndbc.noaa.gov/station_history.php?station=46050

NOAA. 2021f. "Tidal Datums." NOAA Tides & Currents. Accessed April 8, 2021. https://tidesandcurrents.noaa.gov/datum_options.html#NTDE

Oregon Parks and Recreation Department. 2021. "ArcGIS REST Services Directory." Accessed March 19, 2021. https://maps.prd.state.or.us/arcgis/rest/services/Infrastructure/IF_Oregon_Shoreline_Protection_Structures/FeatureServer

Oregon Revised Statutes (ORS). 2019. *State and Local Parks; Recreation Programs; Scenic Waterways; Recreation Trails, ch 390, no. 605 – 770 (2019).* Accessed April 25, 2021. https://www.oregonlegislature.gov/bills_laws/ors/ors390.html

Pilkey, O. H., Wright, H. L. 1988. "Seawalls Versus Beaches." *Journal of Coastal Research* Special Issue (4): 41–64.

Pranzini, E., Wetzel, L., Williams, A. T. 2015. "Aspects of Coastal Erosion and Protection in Europe." *Journal of Coastal Conservation* 19: 445-459.

Pranzini, E., Anfuso, G., Cinelli, I., Piccardi, M., Vitale, G. 2018. "Shore Protection Structures Increase and Evolution on the Northern Tuscany Coast (Italy): Influence of Tourism Industry." *Water* 10 (11): 1647.

Priest, G. R. 1999. "Coastal Shoreline Change Study Northern and Central Lincoln County, Oregon." *Journal of Coastal Research* Special Issue (28): 140–57.

Reguero, B. G., Beck, M. W., Bresch, D. N., Calil, J., Meliane, I. 2018. "Comparing the Cost of Nature-based and Coastal Adaptation: A Case Study from the Gulf Coast of the United States." *PLOS One* 13 (4): 1-24.

Ruggiero, P., List, J. H., 2009. "Improving Accuracy and Statistical Reliability of Shoreline Position and Change Rate Estimates." *Journal of Coastal Research* 25 (5): 1069-1081.

Ruggiero, P., Kratzmann, M.G., Himmelstoss, E.A., Reid, D., Allan, J., Kaminsky, G. 2013. "National assessment of shoreline change—Historical shoreline change along the Pacific Northwest coast" U.S. Geological Survey Open-File Report 2012–1007, 62 p.,

Shih, S.-M., Komar, P. D. 1994. "Sediments, Beach Morphology and Sea Cliff Erosion within an Oregon Coast Littoral Cell." *Journal of Coastal Research* 10 (1): 144–57.

Smith, M. J., Cromley, R. G. 2012. "Measuring Historical Coastal Change using GIS and the Change Polygon Approach." *Transactions in GIS* 16 (1): 3-15.

Stive, M. J. F., Aarninkhof, S. G. J., Hamm, L., Hanson, H., Larson, M., Wijnberg, M., Nicholls, R. J., Capobianco, M. 2002. "Variability of Shore and Shoreline Evolution." *Coastal Engineering* 47: 211-235.

Stockdon, H. F., Sallenger, A. H., List, J. H., Holman, R. A. 2002. "Estimation of Shoreline Position and Change using Airborne Topographic Lidar Data." *Journal of Coastal Research* 18 (3): 502-513.

Sunder, S., Ramsankaran, R, Ramakrishnan, B. 2017. "Inter-comparison of Remote Sensing Sensing-based Shoreline Mapping Techniques at Different Coastal Stretches of India." *Environmental Monitoring and Assessment* 189: 290.

Trenberth, K. 2020. "The Climate Data Guide: Nino SST Indices (Nino 1+2, 3, 3.4, 4; ONI and TNI)." Accessed May 25, 2021. https://climatedataguide.ucar.edu/climate-data/nino-sst-indices-nino-12-3-34-4-oni-and-tni.

United States Department of Agriculture. 2017. *National Agriculture Imagery Program (NAIP) Information Sheet.* Accessed April 2, 2021. https://www.fsa.usda.gov/Assets/USDA-FSA-Public/usdafiles/APFO/support-documents/pdfs/naip_infosheet_2017.pdf

USGS. 2021. "Earth Explorer." USGS Accessed January 21, 2021. https://earthexplorer.usgs.gov

van Rijn, L. C. 2011. "Coastal Erosion and Control." *Ocean & Coastal Management, Concepts and Science for Coastal Erosion Management (Conscience)* 54 (12): 867–87.

Weggel, J. R. 1988. "Seawalls: The Need for Research, Dimensional Considerations and a Suggested Classification." *Journal of Coastal Research*, 29–39.

Xu, H. 2006. "Modification of Normalised Difference Water Index (NDWI) to Enhance Open Water Features in Remotely Sensed Imagery." *International Journal of Remote Sensing* 27 (14): 3025–33.

Appendix A DSAS Summary Report for 1997 - 2016

File name: DSAS_Summary_Transects_two_20210415_213807.txt
Timestamp of rate calculation: 04/15/2021 21:40:13
DSAS version: 5.0.20200527.0200
ArcGIS version: 10.8
Rate types run: SCE, NSM, EPR, LRR, WLR
Baseline layer: BaselineBuffer_Line
Shoreline layer: shorelines
Shoreline dates used: 10/17/1997, 4/27/1998, 9/20/2002, 6/23/2009, 6/15/2012, 7/12/2014, 8/20/2014, 4/28/2016
Shoreline threshold: 0
Confidence Interval (CI) selected: 90
Default Uncertainty: 10
Transect spacing length: 50
Smoothing distance: 100
Coordinate system: NAD_1983_NSRS2007_StatePlane_Oregon_North_FIPS_3601
Is bias applied: YES

All rates reported are in meters/year, distance values are in meters.

DISTANCE: SCE (Shoreline Change Envelope, m)

SCE OVERALL AVERAGES:
total number of transects: 432
average distance: 78.88
maximum distance: 374.79
maximum distance transect ID: 385
minimum distance: 9.49
minimum distance transect ID: 16

DISTANCE: NSM (Net Shoreline Movement, m)

NSM OVERALL AVERAGES:
total number of transects: 432
average distance: 5.18
number of transects with negative distance: 185
percent of all transects that have a negative distance: 42.82%
maximum negative distance: -57.67
maximum negative distance transect ID: 72
average of all negative distances: -17.46
number of transects with positive distance: 247
percent of all transects that have a positive distance: 57.18%
maximum positive distance: 168.47

maximum positive distance transect ID: 226
average of all positive distances: 22.13

RATE: EPR (End Point Rate, m/yr)

EPR OVERALL AVERAGES:
total number of transects: 432
average rate: 0.32
average of the confidence intervals associated with rates: 1.97
reduced n (number of independent transects): 11
uncertainty of the average rate using reduced n: 0.58
average rate with reduced n uncertainty: 0.32 +/- 0.58

number of erosional transects: 185
percent of all transects that are erosional: 42.82%
percent of all transects that have statistically significant erosion: 3.01%
maximum value erosion: -3.55
maximum value erosion transect ID: 134
average of all erosional rates: -0.96

number of accretional transects: 247
percent of all transects that are accretional: 57.18%
percent of all transects that have statistically significant accretion: 9.49%
maximum value accretion: 12.38
maximum value accretion transect ID: 226
average of all accretional rates: 1.29

RATE: LRR (Linear Regression Rate, m/yr)

LRR OVERALL AVERAGES:
total number of transects: 432
average rate: 1.21
average of the confidence intervals associated with rates: 2.86
reduced n (number of independent transects): 24
uncertainty of the average rate using reduced n: 0.58
average rate with reduced n uncertainty: 1.21 +/- 0.58

number of erosional transects: 126
percent of all transects that are erosional: 29.17%
percent of all transects that have statistically significant erosion: 3.24%
maximum value erosion: -3.15
maximum value erosion transect ID: 135
average of all erosional rates: -0.8

number of accretional transects: 306
percent of all transects that are accretional: 70.83%
percent of all transects that have statistically significant accretion: 8.8%
maximum value accretion: 10.57
maximum value accretion transect ID: 385
average of all accretional rates: 2.04

RATE: WLR (Weighted Linear Regression, m/yr)

WLR OVERALL AVERAGES:
total number of transects: 432
average rate: 1.06
average of the confidence intervals associated with rates: 2.98
reduced n (number of independent transects): 25
uncertainty of the average rate using reduced n: 0.6
average rate with reduced n uncertainty: 1.06 +/- 0.6

number of erosional transects: 125
percent of all transects that are erosional: 28.94%
percent of all transects that have statistically significant erosion: 3.47%
maximum value erosion: -3.07
maximum value erosion transect ID: 134
average of all erosional rates: -0.86

number of accretional transects: 307
percent of all transects that are accretional: 71.06%
percent of all transects that have statistically significant accretion: 6.02%
maximum value accretion: 10.21
maximum value accretion transect ID: 385
average of all accretional rates: 1.84

Appendix B DSAS Summary Report for 1997 – 2014

File name: DSAS_Summary_Transects_two_20210421_132716.txt

Timestamp of rate calculation: 04/21/2021 13:28:56

DSAS version: 5.0.20200527.0200

ArcGIS version: 10.8

Rate types run: SCE, NSM, EPR, LRR, WLR

Baseline layer: BaselineBuffer_Line

Shoreline layer: shorelines

Shoreline dates used: 10/17/1997, 4/27/1998, 9/20/2002, 6/23/2009, 6/15/2012, 7/12/2014, 8/20/2014

Shoreline threshold: 0

Confidence Interval (CI) selected: 90

Default Uncertainty: 10

Transect spacing length: 50

Smoothing distance: 100

Coordinate system: NAD_1983_NSRS2007_StatePlane_Oregon_North_FIPS_3601

Is bias applied: YES

All rates reported are in meters/year, distance values are in meters.

DISTANCE: SCE (Shoreline Change Envelope, m)

SCE OVERALL AVERAGES:

total number of transects: 413

average distance: 76.74

maximum distance: 374.79

maximum distance transect ID: 385

minimum distance: 12.76

minimum distance transect ID: 107

DISTANCE: NSM (Net Shoreline Movement, m)

NSM OVERALL AVERAGES:

total number of transects: 413

average distance: 19.71

number of transects with negative distance: 103

percent of all transects that have a negative distance: 24.94%

maximum negative distance: -43.49

maximum negative distance transect ID: 78

average of all negative distances: -13.24

number of transects with positive distance: 310

percent of all transects that have a positive distance: 75.06%

maximum positive distance: 202.59

maximum positive distance transect ID: 244

average of all positive distances: 30.67

RATE: EPR (End Point Rate, m/yr)

EPR OVERALL AVERAGES:

total number of transects: 413

average rate: 1.2

average of the confidence intervals associated with rates: 1.82

reduced n (number of independent transects): 9

uncertainty of the average rate using reduced n: 0.6

average rate with reduced n uncertainty: 1.2 +/- 0.6

number of erosional transects: 103

percent of all transects that are erosional: 24.94%

percent of all transects that have statistically significant erosion: 1.45%

maximum value erosion: -2.7

maximum value erosion transect ID: 134

average of all erosional rates: -0.82

number of accretional transects: 310

percent of all transects that are accretional: 75.06%

percent of all transects that have statistically significant accretion: 32.2%

maximum value accretion: 12.03

maximum value accretion transect ID: 244

average of all accretional rates: 1.88

RATE: LRR (Linear Regression Rate, m/yr)

LRR OVERALL AVERAGES:

total number of transects: 413

average rate: 1.86

average of the confidence intervals associated with rates: 3.08

reduced n (number of independent transects): 19

uncertainty of the average rate using reduced n: 0.7

average rate with reduced n uncertainty: 1.86 +/- 0.7

number of erosional transects: 94

percent of all transects that are erosional: 22.76%

percent of all transects that have statistically significant erosion: 3.63%

maximum value erosion: -2.94

maximum value erosion transect ID: 135

average of all erosional rates: -0.94

number of accretional transects: 319

percent of all transects that are accretional: 77.24%

percent of all transects that have statistically significant accretion: 30.99%

maximum value accretion: 16.91

maximum value accretion transect ID: 385

average of all accretional rates: 2.69

RATE: WLR (Weighted Linear Regression, m/yr)

WLR OVERALL AVERAGES:

total number of transects: 413

average rate: 1.42

average of the confidence intervals associated with rates: 3.29

reduced n (number of independent transects): 20

uncertainty of the average rate using reduced n: 0.73

average rate with reduced n uncertainty: 1.42 +/- 0.73

number of erosional transects: 107

percent of all transects that are erosional: 25.91%

percent of all transects that have statistically significant erosion: 3.63%

maximum value erosion: -2.84

maximum value erosion transect ID: 134

average of all erosional rates: -0.91

number of accretional transects: 306

percent of all transects that are accretional: 74.09%

percent of all transects that have statistically significant accretion: 14.77%

maximum value accretion: 14.13

maximum value accretion transect ID: 385

average of all accretional rates: 2.24